Article

Non-genotoxic transplantation and in vivo selection through epitope editing

https://doi.org/10.1038/s41586-026-10737-8

Received: 30 June 2025

Accepted: 27 May 2026

Published online: 08 July 2026

Open access

Check for updates

Gabriele Casirati[1,2,3,9], Andrea Cosentino[1,2,4,9], Marta Freschi[1,2,4], Jing Zeng[1], Adele Mucci[1,2], Sébastien Levesque[1,2,3], Nola Neri[1], Enrico Drago[1,2,5,6], Viola Carzaniga[1,4], Francesco Romano[1,2], Varun Katta[7], Azusa Matsubara[7], Yichao Li[7], Mohammed S. Mahmoud[1,2,8], Moisés Chávez-Navarro[1,3], Christian Brendel[1,2,3], John P. Manis[1,2,3], Shengdar Tsai[7], Danilo Pellin[1,2,3], Daniel Bauer[1,2,3] & Pietro Genovese[1,2,3]✉

The short-term and long-term effects of genotoxic pre-transplant conditioning remain barriers to the broader application of haematopoietic stem/progenitor cell (HSPC) transplantation and gene therapies[1–4]. Although monoclonal antibodies targeting KIT have been proposed as alternatives to chemotherapy or radiotherapy[5–7], their pharmacokinetics hinder clinical applications owing to the risk of depleting transplanted HSPCs. Here, to address this issue, we identified amino acid changes in the extracellular domain of KIT that disrupt the binding of two therapeutic monoclonal antibodies[8,9], which impair stem cell factor (SCF)-mediated signalling without affecting KIT expression or functionality. We exploited adenine base editing[10] or prime editing[11] to efficiently introduce these mutations in HSPCs and combined them with the disruption of the *BCL11A* erythroid enhancer to promote expression of fetal haemoglobin (HbF)[12,13], a therapeutic approach for several haemoglobinopathies. This strategy enables in vivo co-selection of gene-engineered cells to reach the threshold required to provide therapeutic benefit in patients affected by sickle cell disease and β-thalassaemia. We show progressive enrichment of *KIT* plus *BCL11A* multiplex-edited haematopoiesis under selective pressure with KIT monoclonal antibody, in vitro and in vivo. We report that extended treatment with anti-KIT regimens leads to superior in vivo enrichment while avoiding clonal selection, as assessed by a lentiviral barcoded library. Finally, by overcoming the limitations of monoclonal antibody pharmacokinetics, epitope editing enables novel haematopoietic replacement regimens that are not limited by on-target graft elimination, allowing prolonged immune-based conditioning that maximizes haematopoietic niche clearance without chemo-radiotherapy or monoclonal antibody wash-out.

HSPC transplantation (HSCT) is a cornerstone therapy for a wide range of malignant and non-malignant conditions, leveraging the unique regenerative capacity of HSPCs to replenish the haematopoietic system[14]. Each year, more than 8,000 individuals undergo allogeneic HSCT in the USA, with even more receiving autologous transplants[3,14,15]. The therapeutic potential of HSCT has been further expanded by advancements in gene therapy, which entail the genetic modification of host HSPCs to ameliorate disease phenotypes[16]. However, HSCT carries substantial early and late treatment-related morbidity and mortality[1–4]. Even in patients who surviving more than five years after transplant, mortality remains fourfold to ninefold higher than in the general population[3,17]. The toxicities associated with conditioning regimens, which rely on high-dose chemo- and radiotherapy, are major contributors to these risks[18,19]. Myeloablative agents clear the haematopoietic stem cell (HSC) niche and, in allo-HSCT, contribute to host immunosuppression to overcome immunological barriers[2,20]. However, non-specific genotoxicity has both immediate and long-lasting effects[18,19], including multi-organ damage (to lung, liver, kidney and nervous system) and haematopoietic aplasia, leading to infections, anaemia and bleeding. Survivors face lifelong risk of secondary malignancies, endocrine dysfunction and infertility. Furthermore, inflammation triggered by genotoxic conditioning may increase the risk of graft-versus-host disease[21,22]. These effects disproportionately affect frail individuals with multiple comorbidities and those with advanced malignancies, thereby constraining the broader applicability of HSC therapies.

To overcome these challenges, targeted immunotherapies have been repurposed as safer alternatives to conventional regimens. Monoclonal antibodies (mAbs)[5–7], antibody–drug conjugates (ADCs)[23] and chimeric

[1]Division of Hematology/Oncology, Boston Children's Hospital, Boston, MA, USA. [2]Department of Pediatric Oncology, Dana-Farber Cancer Institute, Boston, MA, USA. [3]Harvard Medical School, Boston, MA, USA. [4]Milano-Bicocca University, Milan, Italy. [5]Clinical and Experimental Immunology, IRCCS Istituto Giannina Gaslini, Genoa, Italy. [6]Department of Neuroscience, Rehabilitation, Ophthalmology, Genetics, and Maternal–Infant Sciences (DINOGMI), University of Genoa, Genoa, Italy. [7]Department of Hematology, St Jude's Children's Research Hospital, Memphis, TN, USA. [8]Zoology Department, Faculty of Science, Fayoum University, Fayoum, Egypt. [9]These authors contributed equally: Gabriele Casirati, Andrea Cosentino. ✉e-mail: Pietro.Genovese@childrens.harvard.edu

antigen receptor (CAR)-T cells[24,25] that recognize the HSC marker KIT (also known as CD117) have been investigated to selectively deplete endogenous HSPCs[26–28]. Such approaches minimize organ damage, shorten aplasia and decrease pro-inflammatory mediators, sparing bone marrow and thymic niches, enabling faster immune recovery[29]. These strategies are particularly suitable for autologous gene therapies, where immune-suppression or complete haematopoietic replacement are not necessarily required. However, immune-based agents pose efficacy and safety challenges due to nonselective targeting of transplanted HSPCs and prolonged half-life, leading to on-target depletion[30,31]. Consequently, transplantation must be delayed until the drug is cleared or sufficiently inactivated. This delay can result in competition between transplanted and host HSPCs, resulting in lower chimerism compared with conventional conditioning[30]. To ensure time-limited HSPC depletion, ADCs with accelerated pharmacokinetics have been used, but these may increase damage to organs that metabolize the toxic payload[32]. Although in certain settings corrected cells have a selective advantage that may compensate for lower engraftment levels[29,33], most genetic diseases require a minimum threshold for correction. For instance, β-haemoglobinopathies, prevalent blood disorders caused by mutations in the β-globin gene (*HBB*), require more than 20% correction for therapeutic benefit[34,35].

We recently showed that precise editing of target epitopes within donor HSPCs confers selective resistance to mAbs or CAR-T cells, without compromising protein function or regulation[36]. Here we leverage this technology to develop a clinically applicable platform for selective engraftment and progressive enrichment of therapeutically gene-modified HSPCs by coupling non-genotoxic immunotherapy-based myeloablation with epitope engineering.

Multiplex editing of KIT and BCL11A

We previously[36] identified mutations in KIT extracellular domain 4 (ECD4) that abrogate the binding of Fab-79D, a mAb that blocks SCF-induced KIT homodimerization[8]. Conversion of histidine 378 to arginine (Fig. 1a and Extended Data Fig. 1a) can be achieved in primary human mobilized peripheral blood-derived CD34$^+$ HSPCs by adenine base editing (ABE), leading to permanent loss of mAb recognition (Fig. 1b) while preserving functionality, engraftment and differentiation capacity[36]. As ABE is well-suited for multiplexing, we combined epitope editing with disruption of the erythroid-specific *BCL11A* enhancer (+58 and +55 sites; Fig. 1c), a strategy to enforce HbF de-repression and improve sickle cell disease (SCD) and transfusion-dependent β-thalassaemia phenotypes[12,13,37]. A similar SpCas9 nuclease strategy (exagamglogene autotemcel (Casgevy)) has recently received approval from the US Food and Drug Administration[38]. After electroporation optimization (Extended Data Fig. 1b), mutiplex base editing of *KIT*^{H378R}, *BCL11A*$^{+58}$ and *BCL11A*$^{+55}$ resulted in efficient editing (78%, 72% and 74%, respectively; Fig. 1d–k and Extended Data Fig. 1c–e), with levels only slightly lower than for individual editing (Fig. 1k). *KIT*^{H378R} plus *BCL11A*$^{+58/+55}$ triplex base editing did not affect the phenotypic composition of CD34$^+$ HSPCs (Fig. 1e), with similar editing across progenitors sorted by fluorescence-activated cell sorting (FACS) and stem-enriched subsets (CD34$^+$CD133$^+$CD45RA$^-$CD90$^+$; Fig. 1f and Extended Data Fig. 1h). In vitro erythroid differentiation confirmed induction of HbF in *BCL11A*-edited cells (Fig. 1g and Extended Data Fig. 1f). Similar to nuclease-mediated disruption[38], dual +58 and +55 targeting by ABE resulted in superior HbF induction compared with individual edits (Fig. 1g). Single-cell FACS confirmed that HbF expression was proportional to the number of disrupted core-half E-box/GATA motifs (TGN$_{7-9}$WGATAR; Fig. 1h). Genomic analyses revealed a large fraction of biallelic edits (78%, 62% and 68% for *KIT*^{H378R}, *BCL11A*$^{+58}$ and *BCL11A*$^{+55}$, respectively; Fig. 1i), which translated to a high rate of *KIT*^{H378R} and *BCL11A*$^{+58/+55}$ co-editing in single cells (Fig. 1j), providing the basis for co-selection.

To characterize their immune resistance, combinations of *KIT*, *BCL11A*$^{+58}$ and *BCL11A*$^{+55}$ base-edited HSPCs (Fig. 1k) were cultured in SCF-containing medium with different Fab-79D concentrations. After 7 days, *KIT*-unedited conditions showed significant growth inhibition, whereas *KIT*^{H378R} cells—alone or combined with *BCL11A* base-edited cells—expanded similarly to untreated cells (Fig. 1l). This protection matched that conferred by SpCas9-mediated *KIT* knockout, which reduced expansion but rendered cells unresponsive to mAb-mediated selection (Extended Data Fig. 1g). Similarly, colony-forming unit (CFU) assays of triplex-edited CD34$^+$ HSPCs plated with or without Fab-79D confirmed growth inhibition of *KIT*-unedited colonies (Fig. 1m,n). Genomic analysis of individual colonies revealed significant co-occurrence of *KIT* and *BCL11A* editing before mAb-mediated selection (Supplementary Table 1). Consistently, exposure to Fab-79D co-enriched editing across all three loci (Fig. 1o). The allelic composition of Fab-79D-treated colonies showed selection of biallelic edits not only for *KIT* but also for *BCL11A*$^{+58}$ and *BCL11A*$^{+55}$ loci (Fig. 1p). These results confirm that base editing-mediated disruption of HbF-repressive elements can be combined with epitope editing in a single ex vivo manipulation, and that multiplex-edited HSPCs can be enriched by antagonistic anti-KIT mAbs.

KIT^{H378R} base editing enables in vivo co-selection

To demonstrate the feasibility of selecting epitope-edited cells in vivo, CD34$^+$ HSPCs edited for *KIT*^{H378R} and *BCL11A*$^{+58/+55}$ were co-injected alongside control *AAVS1*-edited HSPCs in NBSGW mice (Extended Data Fig. 1i). Starting two weeks post-transplant, mice received 8 intravenous doses of Fab-79D (0.5 mg per dose) or PBS. Longitudinal peripheral blood analyses revealed delayed growth of human chimerism in mAb-treated mice, with differences narrowing over the subsequent 14 weeks and becoming negligible at euthanasia (Extended Data Fig. 1j). Fab-79D did not affect lymphoid or myeloid composition (Extended Data Fig. 1k), and multiparametric FACS analysis of bone marrow subsets showed no difference in absolute counts (total cells from hind limbs and sternum) between Fab-79D-treated and mock groups (Extended Data Fig. 1l). However, genomic analysis revealed an approximately twofold increase in *KIT* plus *BCL11A* editing in peripheral blood and bone marrow (Extended Data Fig. 1m,n). To improve detection of lineage-specific effects and effects of non-genotoxic selection on HSC clonality, we designed lentiviral vectors carrying a 28-base degenerate barcode within the 3′ untranslated region (UTR) of constitutively expressed mNeonGreen (mNG) or mTagBFP (mtBFP) cassettes (Fig. 2a). To confirm cell-of-origin tracking, we transduced *KIT*^{H378R} and *AAVS1* base-edited HSPCs with mtBFP or mNG, respectively, which efficiently marked CD34$^+$ progenitors, including stem-enriched fractions (CD34$^+$CD133$^+$CD45RA$^-$CD90$^+$) and enabled discrimination of their progeny (Extended Data Fig. 2a). Competitive in vitro selection, performed by pooling mtBFP-marked *KIT*^{H378R} and mNG-marked *AAVS1* base-edited HSPCs, confirmed that Fab-79D enriched mtBFP$^+$ cells and depleted mNG$^+$ cells (Fig. 2b). Conversely, the balance between non-edited mNG and mtBFP lentivirus-marked cells did not change after challenge with Fab-79D. The absolute count of mtBFP$^+$ *KIT*^{H378R} HSPCs increased despite Fab-79D exposure (Extended Data Fig. 2b), with only the highest dose causing a decrease, probably owing to replacement of medium with mAb volume. To establish efficient in vivo co-selection, we investigated different Fab-79D administration schedules. We hypothesized that prolonged KIT blockade would enhance the depletion of non-edited cells using the same cumulative dose. To test this, NBSGW mice received a pool of *KIT*^{H378R} plus *BCL11A*$^{+58/+55}$ or *AAVS1* base-edited CD34$^+$ HSPCs marked by barcoded mtBFP or mNG lentiviruses, respectively (Fig. 2c). Starting at 6 weeks, mice received 6 doses of Fab-79D (0.5 mg each), according to 3 regimens—dose-dense, every other day; q5d (every 5 days); or q10d (every 10 days)—whereas control mice received PBS. Cumulative Fab-79D exposure was approximately 120 mg kg^{-1}. In vivo selection dynamics was monitored by fluorescent

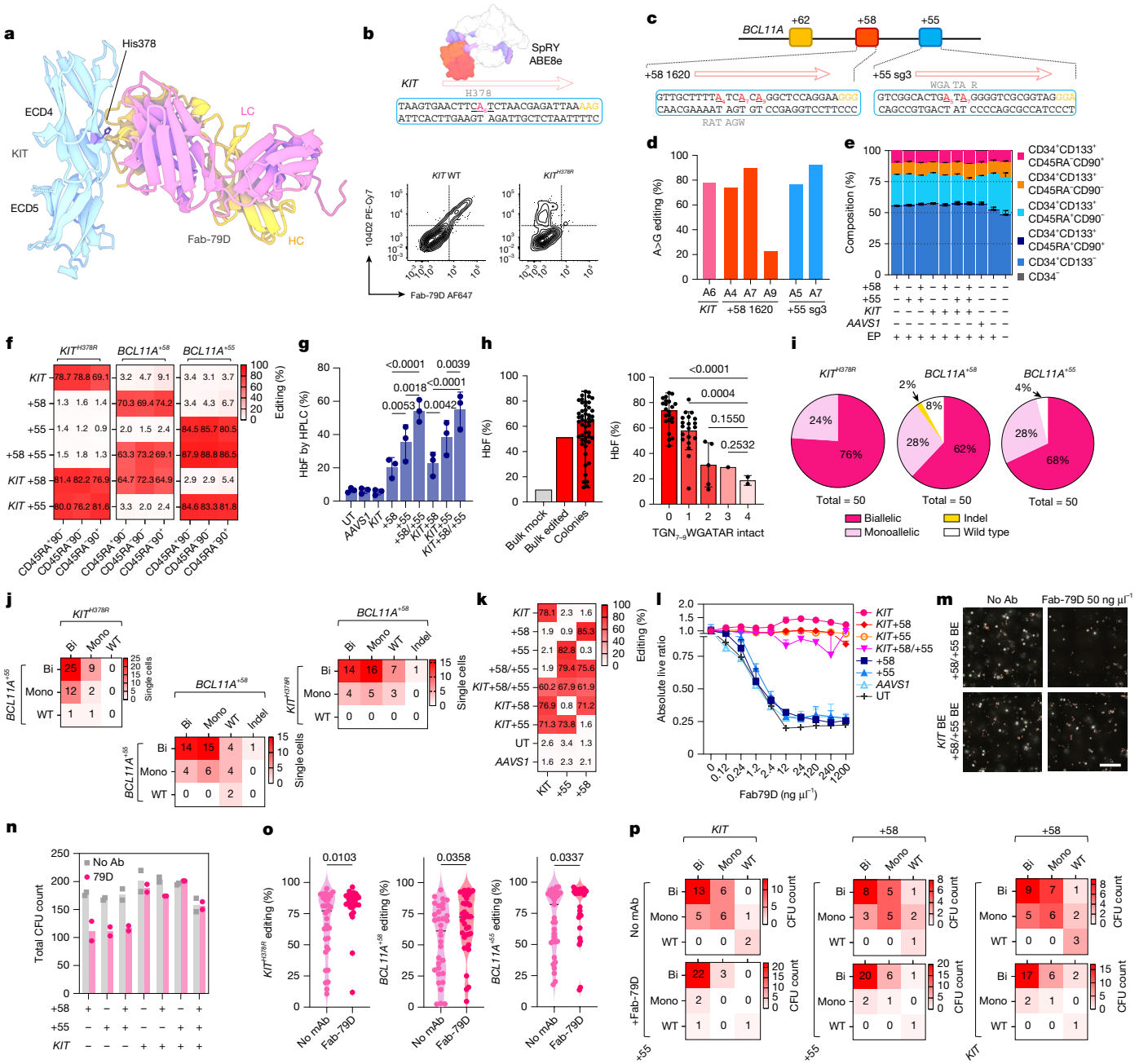

Fig. 1 | Multiplex *KIT* and *BCL11A* base editing enables HbF induction and supports mAb-based selection. a, Structural model (adapted from Protein Data Bank (PDB): 4K9E) of KIT ECD4 bound to Fab-79D. His378 is indicated. HC, heavy chain; LC, light chain. **b**, Top, strategy to introduce the H378R mutation by ABE in exon 7 of *KIT* (structure adapted from PDB: 6VPC). Bottom, representative flow cytometry of bone marrow from NBSGW mice engrafted with unedited or KIT^{H378R} base-edited $CD34^+$ HSPCs stained with Fab-79D and control clone 104D2. **c**, Base editing at the +58 and +55 DNase I hypersensitive sites within the *BCL11A* enhancer. Target edits within WGATAR motifs are highlighted in red. **d**, Representative base-editing efficiencies for KIT^{H378R} and $BCL11A^{+58/+55}$ multiplex editing in HSPCs ($n = 1$). **e**, Phenotypic analysis of edited $CD34^+$ HSPCs. Stacked bars show composition according to CD34, CD133, CD45RA and CD90 expression. Data are mean ± s.d. $n = 3$ donors. EP, electroporation. **f**, Heat maps of editing outcomes across sorted stem and progenitor subsets ($CD45RA^+CD90^-$, $CD45RA^-CD90^-$ and $CD45RA^-90^+$) by editing combinations (left) and sequencing targets (top). $n = 3$ donors. **g**, HbF quantification by HPLC following single or multiplex edits. One-way ANOVA, $Q < 0.05$ indicated. Data are mean ± s.d. $n = 3$ donors. UT, untreated. **h**, HbF quantification after erythroid differentiation of single-cell clones according to the number of disrupted $TGN_{7–9}WGATAR$ motifs. One-way ANOVA, $Q < 0.05$ indicated. Data are mean ± s.d., $n = 50$ clones. **i**,**j**, Single-cell genotyping of edited $CD34^+$ HSPCs, Distribution of monoallelic (Mono), biallelic (Bi) and indel outcomes for KIT^{H378R}, $BCL11A^{+58}$ and $BCL11A^{+55}$ (**i**) and allelic composition heat maps showing frequent biallelic co-editing (**j**). $n = 50$ cells. WT, wild type. **k**,**l**, In vitro selection of multiplex-edited HSPCs using Fab-79D antibody. Baseline editing efficiencies (**k**; $n = 3$ donors) and normalized live $CD34^+$ counts after 7-day culture across mAb doses (**l**; normalized to dose = 0; data are mean ± s.d. $n = 4$ replicates). **m**,**n**, CFU assays plated with or without 50 ng μl^{-1} Fab-79D. Representative images (**m**) and CFU quantification (**n**; $n = 2$; editing conditions as indicated). Scale bar, 5 mm. BE, base editing. **o**,**p**, Single-colony genotyping. Unpaired *t*-test ($P < 0.05$ indicated) (**o**) and allelic composition heat maps of KIT^{H378R}, $BCL11A^{+58}$ and $BCL11A^{+55}$ with or without Fab-79D (**p**). Two-sided *t*-test.

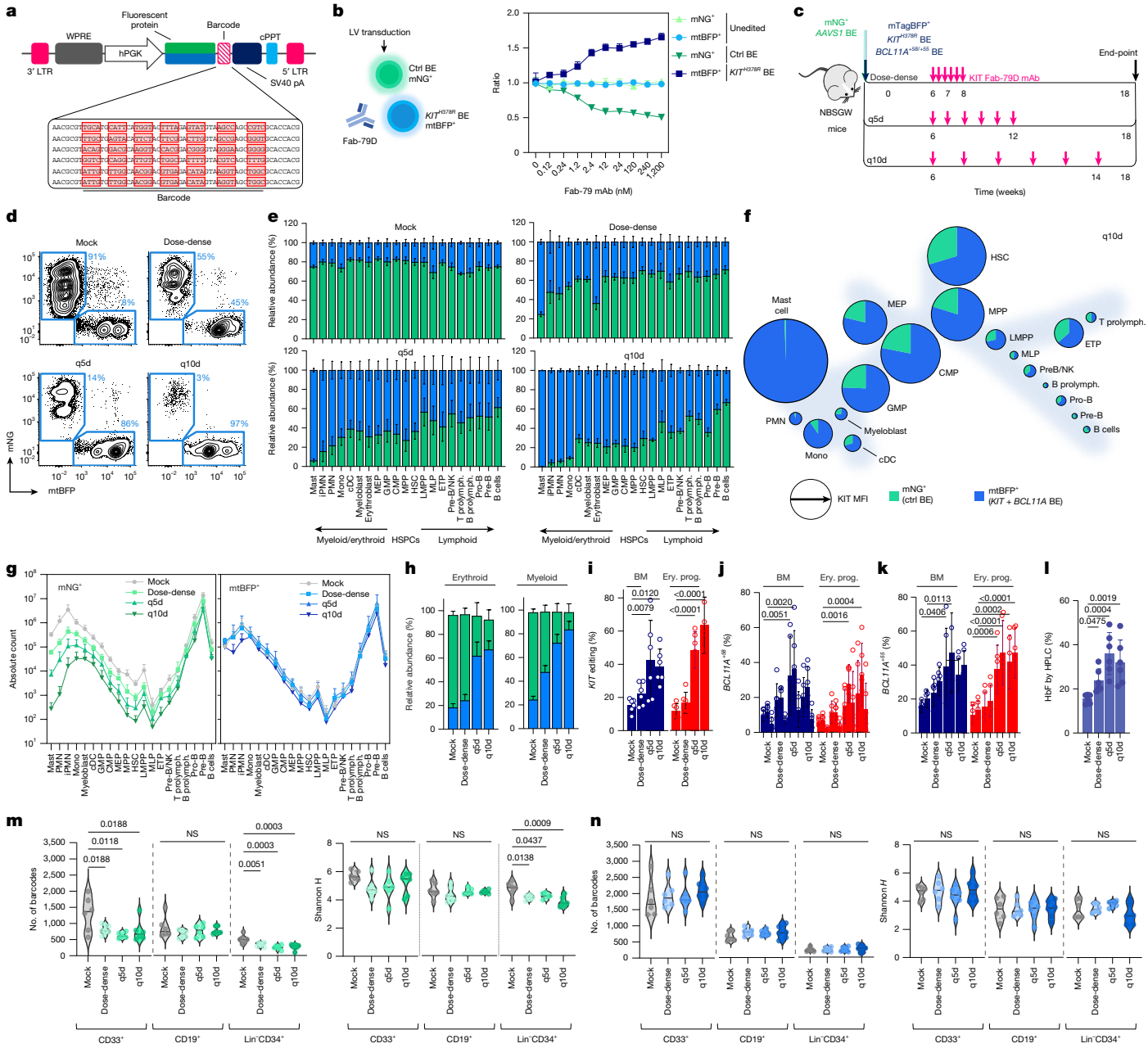

Fig. 2 | In vivo Fab-79D antibody-based co-selection of multiplex-edited HSPCs. a, Lentiviral constructs for HSPC marking and clonal tracking. 7×NNNN bases serve as genomic barcode. cPPT, central polypurine tract; hPGK, human phosphoglycerate kinase promoter; LTR, long terminal repeats; WPRE, woodchuck hepatitis virus post-transcriptional regulatory element. **b**, In vitro competitive assay of *KIT*^{H378R} or *AAVS1* edited or unedited HSPCs transduced with mtBFP or mNG, respectively. Cells were pooled and cultured with Fab-79D at different concentrations. Relative composition after 7 days shows selective advantage of *KIT*^{H378R} (mtBFP$^+$) marked cells. Data are mean ± s.d. $n = 4$ replicates. BE, base-edited; LV, lentivirus. Ctrl, control. **c**, Design of the in vivo competitive transplant selection experiment. NBSGW mice were transplanted with pooled mtBFP$^+$ *KIT*^{H378R} *BCL11A*$^{+58/+55}$ and mNG$^+$ control edited HSPCs. Fab-79D mAb (3 mg cumulative dose) was administered according to different regimens: dose-dense (q2d), q5d and q10d, in addition to a mock group (PBS). $n = 6$ mice per group. **d**, Representative flow plots showing human engraftment and mtBFP$^+$ and mNG$^+$ composition across regimens. **e**, Relative composition across 21 bone marrow haematopoietic subsets at week 18, with mNG$^+$ cells in green and mtBFP$^+$ cells in blue. Data are mean ± s.d. $n = 6$ mice per group. cDC, classical dendritic cells; CMP, common myeloid progenitors; ETP, early T cell progenitors; GMP, granulocyte-monocyte progenitors; iPMN, immature polymorphonuclear granulocyte; LMPP, lymphoid-primed multipotent progenitors; MEP, megakaryocyte-erythroid progenitors; MLP, multi-lymphoid progenitors; mono, monocytes; MPP, multipotent progenitors; PMN, polymorphonuclear granulocyte; pre-B/NK, B and natural killer cell progenitors; prolymph., prolymphocytes. **f**, Subset-resolved selection (q10d cohort). Pie charts show proportions of mtBFP$^+$ and mNG$^+$ cells. Radii are proportional to KIT MFI (mast cell MFI not to scale). **g**, Absolute bone marrow counts of edited (mtBFP$^+$) and control (mNG$^+$) cells across lineages and Fab-79D dosing regimen. Data are mean ± s.d. $n = 6$ mice per group. **h**, Fluorescence composition of erythroid and myeloid colonies derived from bone marrow at end-point. **i**–**k**, Editing efficiencies for *KIT*^{H378R} (**i**), *BCL11A*$^{+58}$ (**j**; from left to right, A4, A7 and A9 target adenines) and *BCL11A*$^{+55}$ (**k**; from left to right, A5 and A7 target adenines) in bulk bone marrow (BM) and their erythroid progeny (Ery. prog.) across regimens (mock, dose-dense, q5d and q10d); Data are mean ± s.d.; one-way ANOVA, $q < 0.05$ indicated. **l**, Quantification of HbF in erythroid progeny by HPLC. One-way ANOVA, $q < 0.05$ indicated. $n = 6$ mice per group. **m**,**n**, Clonality from barcode libraries in FACS-sorted bone marrow subsets (CD33$^+$ myeloid, CD19$^+$ lymphoid and Lin$^-$CD34$^+$ progenitors). Number of barcodes and Shannon diversity index (H) for mNG (**m**) and mtBFP (**n**). One q5d outlier was excluded (ROUT (robust regression and outlier removal) $Q = 1\%$); one-way ANOVA, $q < 0.05$ indicated.

marking of peripheral blood myeloid cells, which readily reflects changes in the progenitor compartment owing to the short half-life of these cells (Extended Data Fig. 2c). In peripheral blood, mtBFP$^+$ cells were progressively enriched from weeks 6 to 13, most prominently in the q5d and q10d groups. At 18 weeks, haematopoietic organs (bone marrow and spleen) were analysed by flow cytometry to assess graft composition (Fig. 2d; gating strategy in Extended Data Fig. 7h). All conditions showed high transduction levels (around 80% mtBFP$^+$ or mNG$^+$ cells among cells expressing human CD45 (hCD45); Extended Data Fig. 2d). Whereas mock-treated mice had a baseline of 21.38 ± 8.9% of mtBFP$^+$ cells, dose-dense, q5d and q10d regimens resulted in increasing enrichment for mtBFP$^+$ cells (37.03 ± 17.03%, 64.54 ± 29.03% and 71.48 ± 20.53%, respectively; Fig. 2e). This observation was also reflected by the absolute counts in human grafts, which were reduced in the mAb-treated cohorts, but only with reduced mNG$^+$ control edited cells (Extended Data Fig. 2d, right). Myeloid and erythroid lineages exhibited higher mtBFP$^+$ fractions compared with lymphoid subsets, with near-complete selection for cells carrying *KIT*^{H378R} plus *BCL11A*$^{+58/+55}$ among mast cells, polymorphonuclear granulocytes and monocytes in the q5d and q10d groups (Fig. 2e and Extended Data Fig. 2e). Although overall KIT expression was maintained (Extended Data Fig. 2f), Fab-79D-mediated selection tracked with surface KIT expression and differentiation dependence across the haematopoietic hierarchy. HSCs, myeloid progenitors and their progeny, which express higher KIT levels, showed a direct correlation between mean fluorescence intensity (MFI) and selection (Fig. 2f and Extended Data Fig. 2h,i). Conversely, lymphoid cells downregulated KIT after the lymphoid-primed multipotent progenitor stage, with differentiated B cells being KIT-negative. This observation is likely to explain the differential enrichment within myeloid and lymphoid lineages in q5d and q10d groups, as these cohorts had shorter intervals between the last mAb dose and euthanasia, highlighting the slower turnover of lymphoid populations. We also observed reduced numbers of control edited mNG$^+$ HSPCs and their myeloid progeny, especially with extended regimens (Fig. 2g). By contrast, mtBFP$^+$ cells showed a minimal reduction compared with mock treatment, consistent with the fraction of *KIT*^{H378R} base-edited HSPCs at the time of transplant. To provide evidence that engrafted HSPCs retain multilineage differentiation after in vivo selection, we performed CFU assays with bulk bone marrow cells. Both erythroid and myeloid colonies retained fluorescent markers similar to HSPCs at the end-point (Fig. 2h). To confirm enrichment at the genomic level and provide a functional readout for *BCL11A* editing, we performed molecular analyses and in vitro erythroid differentiation of bone marrow-derived HSPCs. Editing at all three loci (*KIT*^{H378R}, *BCL11A*$^{+58}$ and *BCL11A*$^{+55}$) was significantly enriched in end-point bone marrow and erythroid progeny (Fig. 2i–k), which translated into HbF de-repression (Fig. 2l). Consistently, the degree of *KIT*^{H378R} genomic editing significantly correlated with the proportion of mtBFP$^+$ HSPCs across treatment cohorts (Extended Data Fig. 2g). Overall, these results show that immunotherapy can enrich multiplex co-edited HSCs and their progeny in vivo, and that prolonged mAb exposure enhances selection outcomes.

In vivo selection does not affect clonality

To assess clonal diversity across haematopoietic lineages within edited (mtBFP$^+$) and unedited (mNG$^+$) haematopoiesis after selection, we sorted CD19$^+$ lymphoid, CD33$^+$ myeloid and lineage$^-$ (Lin$^-$) CD34$^+$ fractions from transplanted mice using FACS and analysed lentivirus genomic barcodes by next-generation sequencing (NGS), which enabled unambiguous barcode quantification (Extended Data Fig. 2j and Supplementary Fig. 1). Analysis of CD19$^+$ cells revealed minimal changes in unique barcode retrieval, Shannon diversity (*H*) and Pielou's evenness (*J*) indexes in mNG$^+$ unedited fractions of mAb-treated and untreated groups (Fig. 2m and Extended Data Fig. 2k), consistent with the relative stability of lymphoid cells (see Fig. 2g). Conversely, in myeloid and Lin$^-$CD34$^+$ populations, the total number of retrieved mNG$^+$ barcodes was significantly decreased across mAb-treated groups (from 1,301 ± 537 and 505 ± 127 in the mock-treated group, to 632 ± 91 and 252 ± 65 in the q5d group, respectively; Fig. 2m). Although unedited HSPC clones were not entirely eliminated even with prolonged treatment regimens, Shannon diversity decreased among mNG$^+$Lin$^-$CD34$^+$ cells in antibody-treated groups, consistent with Fab-79D-mediated growth inhibition of KIT$^+$ progenitors (Fig. 2m, right). By contrast, mtBFP$^+$ multiplex-edited HSPCs (Lin$^-$CD34$^+$) and their CD19$^+$ and CD33$^+$ progeny showed no reduction in unique barcode counts, Shannon diversity or Pielou's evenness, underscoring protection from mAb-mediated depletion conferred by epitope editing (Fig. 2n and Extended Data Fig. 2l).

Overall, these experiments show that multiplex-edited HSPCs can be uniformly enriched by anti-KIT regimens without inducing clonal selection or expansion, with the input number of edited HSCs as well as duration and intensity of antibody conditioning emerging as key determinants of in vivo selection outcomes. The preservation of unedited HSC clones suggests that haematopoietic output may be skewed even with partial host HSC ablation, potentially mitigating risks of graft failure or transplant-related cytopenias.

Epitope editing enables HSPC transplant

To test whether epitope editing enables antibody-mediated replacement of established haematopoiesis, we performed sequential transplantation experiments. Mice were first humanized with HSPCs transduced with the mNG-expressing lentivirus. After confirming engraftment, we administered Fab-79D conditioning (8× 0.5 mg intravenous doses, approximately ~160 mg kg^{-1} cumulative dose) and performed a second transplant of *KIT*^{H378R} or *AAVS1* edited cells. To maximize enrichment, we combined conditioning and selection by administering the second HSPC transplant between the fourth and fifth mAb doses (Extended Data Fig. 3a); mice were euthanized 10 weeks later. Using mNG as a marker of the first unedited donor (90% transduction), we assessed lineage origin by flow cytometry (Extended Data Fig. 3b). Whereas pre-engrafted haematopoiesis was significantly depleted (−72.2% hCD45$^+$mNG$^+$ cells), only mice receiving *KIT*^{H378R} edited cells showed substantial second donor engraftment ($2.86 \times 10^6 \pm 9.32 \times 10^5$ for *KIT*^{H378R} versus $3.93 \times 10^5 \pm 1.58 \times 10^5$ for *AAVS1*; Extended Data Fig. 3c). This led to inversion of the fluorescent composition within the human graft (90% mNG$^+$ to 95% mNG$^-$; Extended Data Fig. 3d). These findings suggest that epitope editing can enable innovative transplantation protocols that are unconstrained by mAb pharmacokinetics, allowing HSPC engraftment close to, or even during, conditioning.

Epitope mapping of the high-affinity SR-1 mAb

Although Fab-79D can select epitope-edited cells in vivo, certain clinical applications may require more complete eradication of host haematopoiesis, particularly when high chimerism is needed or residual host cells are at risk of malignant transformation. To address this, we evaluated different KIT mAbs and identified the SCF-antagonistic SR-1 clone[9] as an ideal candidate. SR-1 competitively blocks SCF and has been clinically evaluated for non-genotoxic conditioning as its humanized aglycosylated counterpart, briquilimab[30,31,39] (ClinicalTrials.gov: NCT05357482[40], NCT06145282, NCT04784052[30] and NCT05903274[39]). SR-1 binds KIT-expressing cells and inhibits expansion of CD34$^+$ HPSCs in vitro at more than tenfold lower concentration than Fab-79D (0.098 ng µl^{-1} and 1.824 ng µl^{-1}, respectively; Fig. 3a,b). Since SR-1 does not recognize mouse KIT, we localized its epitope by screening SR-1 along with other KIT mAbs against human–mouse chimeric KIT constructs in which each extracellular domain (ECD) was replaced by its mouse orthologue (mD1–mD5; Fig. 3c). Loss of staining indicated

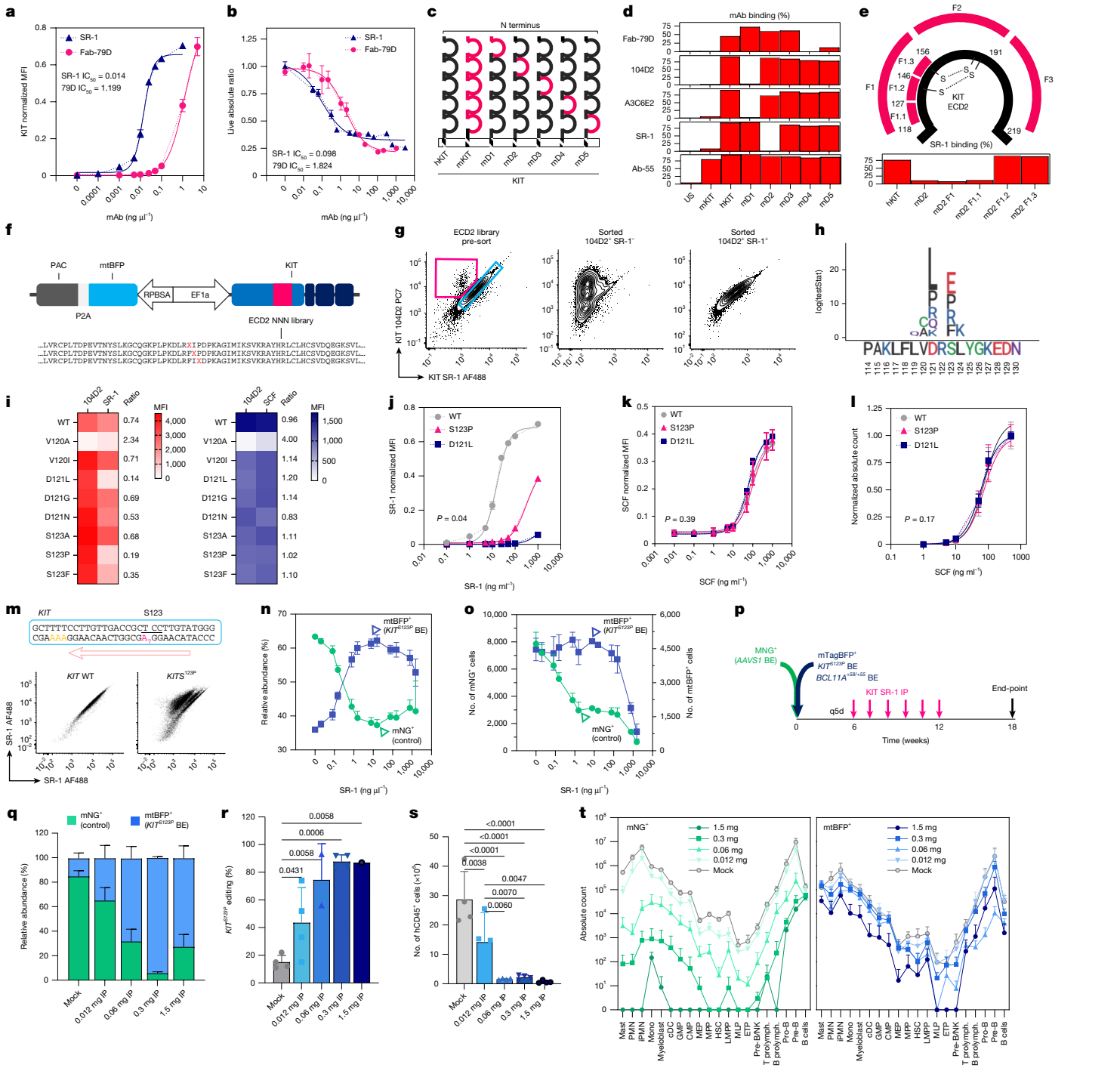

Fig. 3 | Identification of KIT mutations that confer resistance to SR-1. **a**, Affinity of Fab-79D and SR-1 on Ba/F3 cells expressing human KIT. Data are mean normalized MFI ± s.d. $n = 3$; sigmoidal four-parameter logistic curve fitting (4PL). IC_{50}, half-maximal inhibitory concentration. **b**, mAb-mediated growth inhibition in $CD34^+$ HSPCs; normalized absolute counts; $n = 3$ (Fab-79D) and $n = 4$ (SR-1) replicates; data are mean ± s.d.; 4PL. **c**, Mouse:human KIT chimeras for epitope mapping: mouse ECDs are shown in magenta. hKIT, human KIT; mKIT, mouse KIT. **d**, mAb binding across ECD chimeras for Fab-79D, 104D2, A3C6E2, SR-1 and Ab-55. **e**, Fine mapping of SR-1 binding by progressive mouse substitutions. F1, F2 and F3: mouse ortholog fragment 1, 2 and 3, respectively; S–S, disulfide bond. Percent SR-1 binding detected by flow cytometry. **f**, Schematic of mutagenesis library encoding KIT ECD2 with individual degenerate codons. PAC, puromycin *N*-acetyl-transferase reporter casssette. **g**, Flow cytometry of FACS-sorted $SR\text{-}1^+$ $104D2^+$ and $SR\text{-}1^-104D2^+$ fractions. **h**, Logo plot of enriched substitutions in $SR\text{-}1^-$ versus $SR\text{-}1^+$ fractions (amino acids 115–131). **i**, Validation of SR-1 binding (left) and SCF affinity (right) for KIT variants. **j**,**k**, Affinity curves for SR-1 (**j**; $n = 3$) and SCF binding (**k**; $n = 4$) for wild-type KIT and S123P and D121L mutants (MFI normalized to 104D2). Data are mean ± s.d.; 4PL, extra sum-of-squares *F*-test. **l**, Kinase complementation assay on KIT variant-expressing Ba/F3 cells. Absolute counts normalized to [SCF] = 0. Data are mean ± s.d. $n = 4$; 4PL, extra sum-of-squares *F*-test. **m**, ABE strategy to introduce S123P (top) and flow plots of KIT^{S123P} base-edited K562 cells (bottom). **n**–**o**, In vitro competitive assay of KIT^{S123P} versus *AAVS1* base-edited HSPCs cultured with SR-1. Relative (**n**; $n = 4$) and absolute (**o**; $n = 4$) counts of $mtBFP^+$ (KIT^{S123P}) (blue) and mNG^+ (*AAVS1*-edited) (green) cells. Data are mean ± s.d. **p**, In vivo SR-1 dosing experiment. NBSGW mice were transplanted with KIT^{S123P} plus $BCL11A^{+58/+55}$ ($mtBFP^+$) and control (mNG^+) base-edited HSPCs. **q**, Relative $mtBFP^+$ and mNG^+ composition in human grafts with different intraperitoneal (IP) doses of SR-1. Data are mean ± s.d. $n = 4$ mice per group. **r**, KIT^{S123P} editing efficiency in bone marrow at end-point with different doses of SR-1. **s**,**t**, Engraftment and lineage output. Total $hCD45^+$ bone marrow cells (**s**) and absolute counts across haematopoietic subsets (**t**) at end-point. Data are mean ± s.d. $n = 4$ mice per group. One-way ANOVA, $q < 0.05$ indicated.

that SR-1 primarily binds ECD2 (Fig. 3d). In line with this observation, *KIT*^{H378R} (which is mutated in ECD4), did not confer protection to HSPCs cultured with SR-1 (Extended Data Fig. 3e). Progressive restriction of the chimeric region narrowed the SR-1 epitope to positions 118–127 (Fig. 3e). To identify single point mutations, we designed a degenerate codon library spanning ECD2 (Fig. 3f) and screened it using SR-1 and 104D2, which binds a non-overlapping epitope on ECD1 (Fig. 3g). NGS of FACS-sorted SR-1$^-$ and SR-1$^+$ cells revealed amino acid substitutions at two positions within the mapped interval (Extended Data Fig. 3f), prompting the validation of selected variants at 121 and 123 (Fig. 3h,i). By assessing loss of SR-1 recognition, preservation of KIT expression, and SCF-binding capacity (Fig. 3i), D121L and S123P emerged as the most promising candidates, the latter corresponding to a mouse orthologue residue. Affinity analysis showed near-complete loss of SR-1 recognition for D121L, whereas S123P retained partial binding at high concentrations (>100 ng μl^{-1}; Fig. 3j). Neither mutation altered SCF affinity, which remained similar to that of the wild type (Fig. 3k), nor SCF-induced proliferation in mouse IL-3-dependent Ba/F3 cells transduced with human KIT variants and exposed to human SCF (Fig. 3l). These data support the development of SR-1 epitope editing at D121 or S123 positions without disruption of the SCF–KIT ligand-receptor interaction.

S123P confers partial resistance to SR-1

Given the efficiency and multiplexing potential of base editing, we first assessed installation of the S123P mutation by ABE. Using our K562 reporter line, which overexpresses KIT from the endogenous locus[36], we selected the best-performing single guide RNA (sgRNA) to efficiently introduce S123P (Extended Data Fig. 3g,h) and tested it in CD34$^+$ HSPCs, achieving an editing efficiency of about 75% (Fig. 3m and Extended Data Fig. 3i). sgRNA_3 provided the highest efficiency, but introduced non-silent bystander mutations at positions L124 and Y125. Conversely, sgRNA_1 displayed marginally lower editing (60%) but generated a silent bystander (A11, Extended Data Fig. 3i). We next evaluated whether *KIT*^{S123P} HSPCs were protected from SR-1-mediated SCF blockade in vitro. In competitive cultures, *KIT*^{S123P} base-edited HSPCs labelled with mtBFP were pooled with control *AAVS1* base-edited cells labelled with mNG. Challenge with increasing SR-1 concentrations enriched mtBFP$^+$ HSPCs, plateauing at 10–100 ng μl^{-1} SR-1 (Fig. 3n). At concentrations greater than 100 ng μl^{-1}, the relative selection for *KIT*^{S123P} waned, probably reflecting mAb-mediated depletion regardless of editing status, as supported by decreased absolute counts of both mtBFP$^+$ and mNG$^+$ cells (Fig. 3o). We therefore evaluated whether SR-1 dose titration could uncover a therapeutic window for in vivo selection of *KIT*^{S123P} haematopoiesis. mtBFP-marked *KIT*^{S123P} plus *BCL11A*$^{+58/+55}$ base-edited HSPCs were pooled with mNG-marked *AAVS1* base-edited HSPCs and competitively transplanted into NBSGW mice (Fig. 3p). After 6 weeks, mice received 6× weekly intraperitoneal administrations of SR-1, based on the superior performance of prolonged mAb regimens. We tested 4 dosages of SR-1 (cumulative doses 0.012 mg, 0.06 mg, 0.3 mg and 1.5 mg, corresponding to 0.48 mg kg^{-1}, 2.4 mg kg^{-1}, 12 mg kg^{-1} and 60 mg kg^{-1}), in addition to PBS control. Eighteen weeks after transplant, mock-treated mice showed a median of 12.63% mtBFP$^+$ cells across haematopoietic bone marrow subsets (Fig. 3q). SR-1-treated cohorts showed dose-dependent selection of mtBFP$^+$ haematopoiesis, which was nearly complete at doses of 0.3 mg and higher (Fig. 3q). As with Fab-79D, selection was lineage-dependent, with myeloid subsets being preferentially derived from mtBFP$^+$ progenitors, whereas lymphoid cells tended to retain a mNG$^+$ origin (Extended Data Fig. 3J). Molecular analyses confirmed efficient selection of *KIT*^{S123P} (Fig. 3r). Despite this, quantitative analyses showed that mtBFP$^+$ enrichment was associated with a marked decrease in the absolute number of human cells (Fig. 3s,t). At doses lower than 0.3 mg, this decrease aligned with the low input fraction of transplanted mtBFP$^+$ cells (around 13%). However, at higher doses, graft composition and absolute counts indicated that *KIT*^{S123P} HSPCs and their progeny were incompletely protected. We concluded that *KIT*^{S123P} base editing enables enrichment of engineered cells and enhances the therapeutic index of the SR-1, but careful dosing is essential to ensure shielding of edited cells.

KIT^{D121L} prevents SR-1-mediated depletion

Since *KIT*^{D121L} showed lower residual SR-1 binding than *KIT*^{S123P} (Fig. 3j) but could not be installed by adenine or cytidine base editing, we utilized a prime-editing[11] approach and leveraged the PE7 configuration[41], which incorporates the RNA-binding protein La to enhance prime-editing guide RNA (pegRNA) stability. To install *KIT*^{D121L}, we designed a pegRNA that maximized C•C mismatches at the targeted triplet and introduced neighbouring silent mutations to evade mismatch repair (Fig. 4a and Extended Data Fig. 4a,b). *KIT* pegRNA was co-delivered with our *BCL11A*$^{+58}$-disrupting pegRNA[42] to achieve double editing and enable co-selection (Fig. 4b). After optimizing electroporation for prime editing delivery in human HSPCs (Extended Data Fig. 4c), we evaluated different culture media formulations to improve editing, viability and maintenance of stem cell phenotype (Extended Data Fig. 4d–i). X-VIVO15 medium yielded the highest editing efficiencies (Extended Data Fig. 4f), which were associated with higher expression of a co-electroporated spike-in eGFP mRNA (Extended Data Fig. 4h,i), but significantly reduced the stem-enriched CD45RA$^-$CD90$^+$ fraction compared with SFEMII medium (Extended Data Fig. 4f). We thus selected SFEMII and the cytokine combination that produced the highest absolute number of edited CD45RA$^-$CD90$^+$ cells, potentially maximizing engrafting HSC numbers and clonal diversity. To enhance reverse transcription for prime editing, we exploited deoxynucleoside supplementation (dNS) and Vpx mRNA co-delivery[42], which further increased *KIT* and *BCL11A*$^{+58}$ editing (Extended Data Fig. 4j). Using an optimized PE3 design, we achieved up to 55% *KIT* and 75% *BCL11A* editing (Fig. 4c). After erythroid differentiation, *BCL11A*$^{+58}$ prime editing induced robust HbF expression, with consistently higher levels with PE3 than PE2 (Fig. 4d). The *BCL11A*$^{+58}$ prime-editing strategy resulted in greater HbF induction than *BCL11A*$^{+58}$ base editing at similar editing rates (Figs. 1g and 4c,d), possibly owing to different base changes within the WGATAR motif or occurrence of PE3-associated insertion–deletion mutations (indels). To assess monoallelic versus biallelic *BCL11A*$^{+58}$ disruption, we performed erythroid differentiation from individually sorted prime-edited CD34$^+$ HSPCs. *BCL11A*$^{+58}$ PE3 produced more biallelic edits than PE2 (Fig. 4e), resulting in more robust HbF induction (Fig. 4d–f). As with base editing, prime editing did not skew stem and progenitor cell composition (Fig. 4g) or impair HSPC expansion in SCF-containing culture (Extended Data Fig. 4k). Phosphoflow analysis[36] of *KIT*^{D121L} HSPC-derived myeloid cultures confirmed preserved responses to multiple stimuli compared with unedited cells (Extended Data Fig. 4l and Supplementary Information 6 and 7). RNA-sequencing (RNA-seq) analysis of HSPCs edited at *KIT*^{D121L}, *BCL11A*$^{+58}$ or *AAVS1* using PE2 or PE3 and stimulated with SCF produced the expected SCF-induced transcriptional response in all conditions (Extended Data Fig. 4m–o), with no discernible alterations attributable to *KIT*^{D121L} editing (Extended Data Fig. 4p). Notably, *KIT*^{D121L} and *BCL11A*$^{+58}$ prime-editing outcomes were similar across FACS-sorted progenitors and stem-enriched subsets, regardless of Vpx co-transfection or PE2 or PE3 design (Fig. 4h). We next assessed protection of prime-edited HSPCs from SR-1 in vitro. As observed for *KIT*^{H378R} and Fab-79D, *KIT*^{D121L} endowed CD34$^+$ cells with selective resistance to SR-1-mediated SCF blockade proportional to editing efficiency (54 ± 3.3%). This protection persisted even at the highest dose (Fig. 4i), thereby improving upon S123P mutation (Fig. 3n,o). *KIT*^{D121L} conditions retained higher CFU counts than unedited counterparts exposed to SR-1 (Fig. 4j). As with base editing, editing rates for both *KIT*^{D121L} and *BCL11A*$^{+58}$ increased in a SR-1 dose-dependent manner among CFUs derived from multiplex prime-edited HSPCs (Fig. 4k), suggesting that both editing technologies produce non-independent co-editing of different loci within the same cells, thereby minimizing

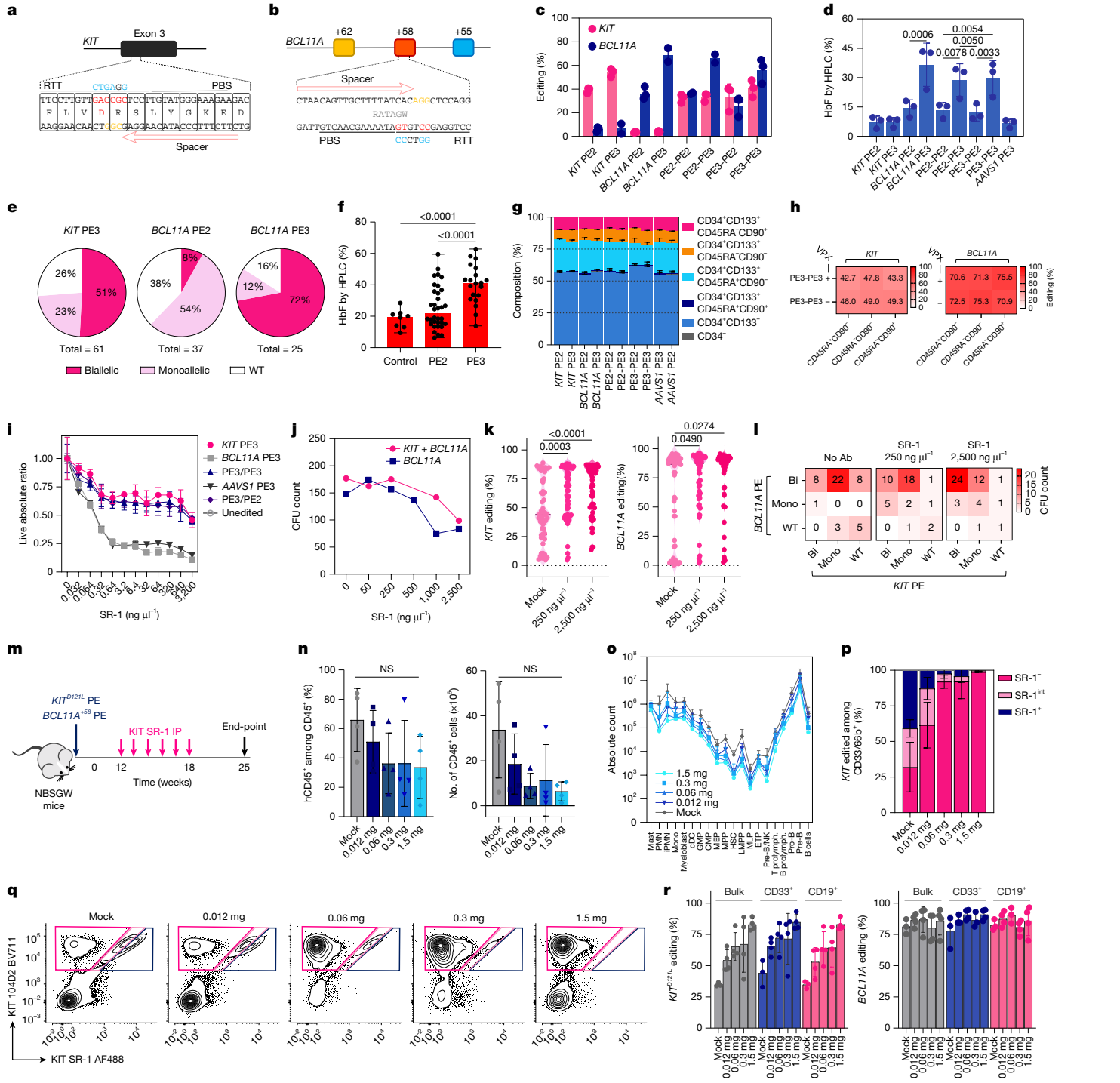

Fig. 4 | See next page for caption.

enrichment of *KIT*-only edited cells. Allelic analysis of individual CFUs showed that SR-1 exposure up to 250 ng µl^{-1} mostly depleted cells with wild-type *KIT* while preserving *KIT*^{D121L} monoallelic edits, whereas higher doses specifically enriched for biallelic edits (Fig. 4l).

Genomic safety of *KIT* and *BCL11A* editing

Prime editing is considered a high-fidelity genome-engineering approach; however, PE3 can introduce DNA double-strand breaks through second-strand nicking, potentially generating indels. To quantify editing purity, we performed NGS of the *KIT* and *BCL11A* loci in prime-edited HSPCs and in vitro differentiated erythroid cells (Extended Data Fig. 5a–d). At *KIT*, indels were negligible with PE2 (0.02 ± 0.01% and 0.013 ± 0.015% for HSPCs and erythroid progeny, respectively), whereas PE3 produced higher indel rates (4.06% and 2.05%, respectively). By contrast, *BCL11A* PE3 generated substantially higher indel frequencies, up to 44.8% and 25.2%, compared with 5.28% and 1.51% for PE2 in HSPCs and erythroid progeny, respectively, probably reflecting the short distance between the pegRNA and nicking guide (29 nt). Although these findings may raise concerns, *BCL11A*$^{+58}$ enhancer-disrupting indels still contribute to therapeutic effect. We next evaluated genomic off-target profiles of our genome-editing strategies. Candidate off-target sites were nominated using complementary approaches: GUIDE-seq[43], CHANGE-seq-BE[44]

Fig. 4 | Prime editing enables *KIT* epitope editing and *BCL11A* erythroid enhancer disruption and enhances in vivo selection by SR-1. a,**b**, Design of prime editing to install KIT^{D121L} (**a**) and disrupt the DNase I hypersensitive site at *BCL11A* +58 (WGATAR) (**b**). PBS, primer-binding site; RTT, reverse transcription template. **c**, Multiplex *KIT* plus *BCL11A* prime editing efficiencies using PE2 and/or PE3 designs. Data are mean ± s.d. $n = 3$ donors. **d**, Detection of HbF by HPLC in erythroid progeny from **c**. One-way ANOVA, $q < 0.05$ indicated. Data are mean ± s.d. $n = 3$ donors. **e**, Allelicity distributions at KIT^{D121L} and $BCL11A^{+58}$ for PE2 or PE3 designs. **f**, HbF in erythroid progeny from single-cell–derived clones edited with PE2 or PE3. Data are mean ± s.d. $n = 8$, 34 and 20 for control, PE2 and PE3, respectively. **g**, Immunophenotype of edited $CD34^+$ HSPCs. Data are mean ± s.d. $n = 3$ donors. **h**, Heat map of editing across FACS-sorted progenitors ($CD45RA^+CD90^-$, $CD45RA^-CD90^-$ and $CD45RA^-CD90+$) with or without Vpx mRNA. $n = 3$ replicates. **i**, Growth inhibition of KIT^{D121L} and/or $BCL11A^{+58}$ prime-edited HSPCs by SR-1. Absolute counts normalized to dose = 0. Data are mean ± s.d. $n = 4$. **j**, Total CFU counts for KIT^{D121L} and/or $BCL11A^{+58}$ prime-edited HSPCs exposed to SR-1. Data are mean ± s.d. $n = 2$. **k**,**l**, Single-colony genotyping after SR-1 treatment (250–2,500 ng μl^{-1}): editing efficiencies for KIT^{D121L} and $BCL11A^{+58}$ (**k**; one-way ANOVA ($q < 0.05$)) and heat map of allelic distribution (**l**). **m**, In vivo dosing experiment. Mice were treated with 6× weekly intraperitoneal doses of SR-1 (cumulative dose 0.012–1.5 mg). $n = 4$ mice per group. PE, prime editing. **n**, Human cell engraftment in bone marrow at end-point: percentage of $hCD45^+$ cells (left) and absolute counts (right). Data are mean ± s.d. $n = 4$ mice per group, one-way ANOVA. **o**, Absolute counts of human haematopoietic subsets in bone marrow with different doses of SR-1. Data are mean ± s.d. $n = 4$ mice per group. **p**,**q**, In vivo epitope editing outcomes. Dual SR-1 plus 104D2 staining in $CD33/66b^+KIT^+$ myeloid cells showing wild-type ($SR\text{-}1^+$), monoallelic (intermediate) and biallelic ($SR\text{-}1^-$) fractions (**p**), with representative flow plots showing the $CD33/66b^+CD14\text{-}SSC^{hi}$ fraction (**q**). Fractions are highlighted as follows: biallelic-edited, magenta; monoallelic, light pink; and unedited, blue. Data are mean ± s.d. $n = 4$ mice per group. **r**, Genotyping of KIT^{D121L} prime editing and $BCL11A^{+58}$ prime editing in bulk bone marrow and sorted $CD33^+$ (myeloid) or $CD19^+$ (lymphoid) compartments. Data are mean ± s.d. $n = 4$ mice per group.

(Supplementary Figs. 2 and 3), and in silico prediction (CRISPOR[45]) for base editing; CHANGE-seq (Supplementary Figs. 3–5) and CRISPOR for prime-edited pegRNAs and nicking sgRNAs. For CHANGE-seq, the top 30 non-intergenic sites shared across 2 replicates were selected. For GUIDE-seq, top non-intergenic sites with fewer than eight mismatches and NRN protospacer-adjacent motifs (PAMs) were prioritized. These candidates were incorporated into rhAmpSeq panels comprising 193 and 111 base-editing and prime-editing sites, respectively (Supplementary Table 6), and analysed by NGS in edited HSPCs from three donors. Consistent with prior reports, prime editing did not induce detectable off-target base substitutions (Extended Data Fig. 5f). By contrast, SpRY-ABE8e base editing produced measurable off-target deamination (positions 1–10) at several loci, most prominently for the $BCL11A^{+58}$ sgRNA (Extended Data Fig. 5e and Supplementary Tables 7–9). rhAmpSeq confirmed on-target indel frequencies consistent with those observed by locus-specific sequencing (Extended Data Fig. 5a–d) and detected no indels at off-target sites (Extended Data Fig. 5f).

Given the non-negligible indel incidence with PE3, we assessed the possibility of genomic translocations between *KIT* and *BCL11A*. We first implemented screening with uni-directional targeted sequencing (UDiTaS[46]) for *KIT*, $BCL11A^{+55}$ and $BCL11A^{+58}$ sites (Extended Data Fig. 5g–i). No rearrangements were detected (≥1% threshold) in triplex base-edited HSPCs (Extended Data Fig. 5h and Supplementary Table 11). However, in 2 out of 3 PE3-edited donors, UDiTaS revealed evidence of translocations, including one event involving the on-target sites on chromosomes 2 and 4 (Extended Data Fig. 5j). To quantify on-target translocations, we optimized PCR assays for *KIT*–*BCL11A* rearrangements using 'short' or 'long' amplicons and validated them in SpCas9 nuclease-treated K562 cells, which generated translocation products that confirmed assay sensitivity (Extended Data Fig. 6a–e). We then applied short-amplicon assays to $CD34^+$ HSPCs across multiple gRNA plus nuclease combinations, as controls, and the *KIT* plus *BCL11A* PE3-PE3 condition, which produced detectable bands (Extended Data Fig. 6f,g). For quantitative analysis, we developed digital droplet PCR (ddPCR)-assays using primers combinations targeting *KIT*–*BCL11A* rearrangements in every orientation (Extended Data Fig. 6h,i). Specificity and sensitivity were benchmarked using PCR products from nuclease-treated cells (Extended Data Fig. 6g,h), which were re-sequenced to confirm bona fide *KIT*–*BCL11A* breakpoints. In $CD34^+$ HSPCs, SpCas9 nuclease treatment produced relatively high translocation frequencies (0.98 ± 0.39 and 1.16 ± 0.38 events per 1,000 diploid genomes for KIT_Fw–BCL11A_Rv and KIT_Rv–BCL11A_Fw amplicons, respectively). PE3 showed a trend toward increased translocation frequency (0.16 ± 0.02 and 0.13 ± 0.04, for Fw-Rv and Rv-Fw, respectively) relative to PE2 (0.02 ± 0.04 and 0.09 ± 0.08) or unedited controls (0.02 ± 0.04 and 0.02 ± 0.04; Extended Data Fig. 6i).

Collectively, these analyses provide an in-depth genomic safety assessment of KIT-BCL11A multiplex base editing and prime editing-based strategies. *KIT* epitope editing showed an excellent safety profile for both mutations (H378R and D121L), even with PAM-flexible Cas9 variants. By contrast, *BCL11A* targeting was associated with off-target deamination with base editing and on-target indels with PE3. Although current designs prioritized maximal efficiency for proof-of-concept studies, future clinical translation will benefit from further optimization of editor–guide combinations, including PAM-restricted Cas variants to reduce *BCL11A* base-edited off-target activity and optimization of prime editing configurations to achieve efficient editing with PE2 systems, thereby minimizing risk of double-strand breaks.

KIT^{D121L} cells are enriched in vivo by SR-1

We next assessed the in vivo protection conferred by KIT^{D121L} prime editing. NBSGW mice were xenografted with KIT^{D121L} plus $BCL11A^{+58}$ dual prime-edited HSPCs (Fig. 4m) and, after steady-state engraftment, treated them with a 6-dose SR-1 regimen as in Fig. 3n (0.012 to 1.5 mg). At end-point, both the fraction and absolute counts of bone marrow $hCD45^+$ cells decreased (Fig. 4n) uniformly across all lineages (Fig. 4o). This reduction was partial at the lowest dose but, as the dose increased, it approached a plateau consistent with *KIT* editing in the input HSPCs (approximately 36%), suggesting selective depletion of unedited cells. Even at the highest dose, SR-1-mediated depletion was less severe than previously observed with KIT^{S123P} (Fig. 3q–t), highlighting the increased therapeutic index conferred by KIT^{D121L} (Fig. 4o). By co-staining bone marrow cells with SR-1 and clone 104D2, we identified wild-type, monoallelic and biallelic edited cells within the myeloid progeny (Fig. 4p,q). We observed a dose-dependent elimination of wild-type *KIT* and monoallelic-edited cells, with only SR-1-negative cells persisting at higher doses (Fig. 4q). Genomic analysis confirmed dose-dependent selection of *KIT* prime-edited cells in bulk bone marrow and FACS-sorted $CD19^+$ and $CD33^+$ subsets (Fig. 4r). Owing to the high-input $BCL11A^{+58}$ editing, we were unable to confirm co-enrichment in this non-competitive transplant setting.

KIT^{D121L} enables efficient HSCT

To demonstrate how KIT^{D121L} prime editing could improve non-genotoxic transplantation protocols, we modelled HSCT with SR-1 immune conditioning. NBSGW mice were pre-engrafted with unedited mNG-transduced HSPCs, monitored until full human engraftment, and then conditioned with two intravenous SR-1 doses (2× 0.25 mg or 2× 0.5 mg). Twelve hours after the second dose, mice received $mtBFP^+$ HSPCs with $BCL11A^{+58}$ or KIT^{D121L} plus $BCL11A^{+58}$ prime editing (Fig. 5a).

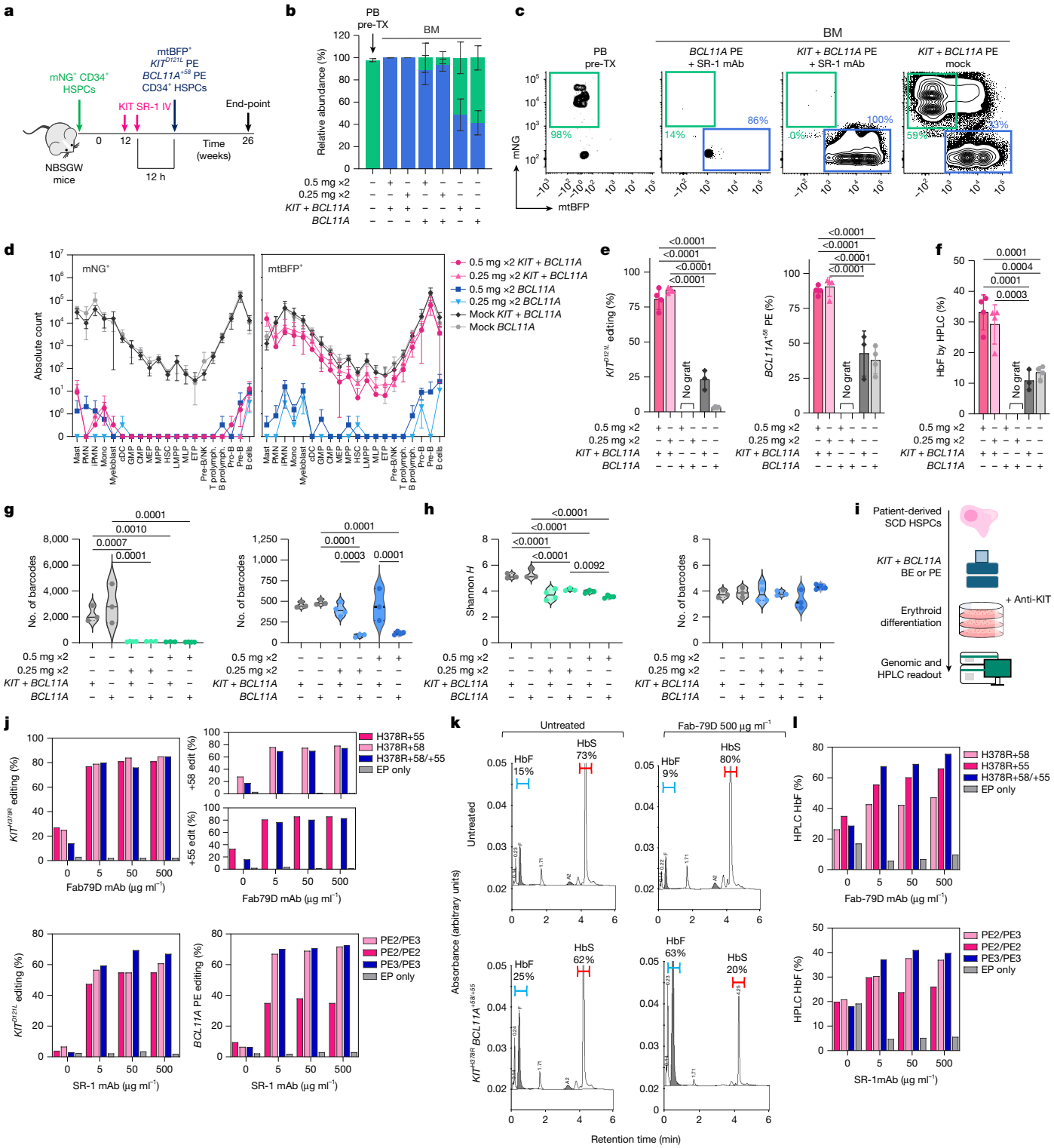

Fig. 5 | See next page for caption.

Unlike current non-genotoxic conditioning trials, this short interval was chosen to simulate early transplantation without mAb wash-out. In the *KIT*^{D121L} plus *BCL11A*$^{+58}$ group, we confirmed near-complete eradication of the first mNG^{+} graft and establishment of an entirely mtBFP^{+} second graft (Fig. 5b,c). Conversely, withholding mAb conditioning produced mixed chimerism regardless of editing (around 50% mNG^{+}; Fig. 5b). Critically, in the *BCL11A*$^{+58}$ prime-edited group, the absolute number of engrafted cells was negligible (Fig. 5d), highlighting that, as intended, residual SR-1 levels were sufficient to eradicate the first graft and prevent engraftment of non-epitope-edited HSPCs. Remarkably, *KIT*^{D121L} plus *BCL11A*$^{+58}$ prime-edited HSPCs produced a multilineage graft even in this challenging setting. Genomic analysis confirmed selective engraftment of *KIT*^{D121L} prime-edited cells and co-selection for *BCL11A*$^{+58}$ (Fig. 5e), resulting in efficient HbF induction after erythroid differentiation (Fig. 5f). Owing to low residual cell numbers after mAb depletion, genomic and functional readouts could not be completed for the *BCL11A*$^{+58}$ prime-edited condition. NGS revealed significant loss of total retrieved barcodes and Shannon diversity among mNG-marked

Fig. 5 | *KIT*^{D121L} epitope editing enables non-genotoxic haematopoietic replacement and selection of *BCL11A*-edited SCD progenitors. a, In vivo haematopoietic replacement experiment. NBSGW mice pre-engrafted with mNG$^+$ unedited HSPCs received SR-1 conditioning (2 doses) and, after 12 h, were transplanted with mtBFP$^+$ *BCL11A*$^{+58}$ or *BCL11A*$^{+58}$ plus *KIT*^{D121L} prime-edited HSPCs. $n = 4$ per group. IV, intravenous injection. **b**, Relative mNG (green) and mtBFP (blue) composition of hCD45$^+$ cells across time points or groups. BM, end-point bone marrow; PB pre-TX, pre-treatment peripheral blood. Data are mean ± s.d. **c**, Representative flow plots (bi-exponential axis) of hCD45$^+$ cells in pre-treatment peripheral blood and in bone marrow at end-point. **d**, Absolute bone marrow counts of mtBFP$^+$ and mNG$^+$ human haematopoietic subsets following SR-1 conditioning and haematopoietic replacement. Data are mean ± s.d. $n = 4$ mice per group. **e**, End-point genotyping of *KIT*^{D121L} and *BCL11A*$^{+58}$. Data are mean ± s.d. $n = 4$ mice per group. One-way ANOVA, $q < 0.05$. **f**, HbF expression after erythroid differentiation of end-point bone marrow cells, determined by HPLC. Data are mean ± s.d. $n = 4$ mice per group. One-way ANOVA, $q < 0.05$. **g**,**h**, Clonality of the human graft in bone marrow. Number of retrieved barcodes (**g**) and Shannon *H* index (**h**). One-way ANOVA, $q < 0.05$ indicated. **i**, Experimental design to edit and select for *KIT* epitope and *BCL11A*-edited HSPCs from a patient with SCD. **j**, Editing efficiencies for *KIT* and *BCL11A* in erythroid cultures exposed to different concentrations of Fab-79D or SR-1. EP, electroporation only. **k**, Representative haemoglobin HPLC of SCD-derived erythroid cells under anti-KIT mAbs (Fab-79D or SR-1) at indicated doses; unedited and triplex *KIT*^{H378R}, *BCL11A*$^{+58}$ plus *BCL11A*$^{+55}$ base-edited conditions are shown (with or without 500 μg ml^{-1} Fab-79D). HbF and HbS peaks are labelled with the respective per cent composition. **l**, HbF quantification in differentiated erythroid cells from **i**–**k** by HPLC.

cells in mice receiving either SR-1 dose (Fig. 5g,h). Consistent with SR-1 susceptibility, the *BCL11A*$^{+58}$ prime-edited group also showed negligible barcode counts compared with the no-conditioning control. Conversely, *KIT*^{D121L} plus *BCL11A*$^{+58}$ prime-edited groups preserved barcode numbers and Shannon diversity regardless of SR-1 conditioning (Fig. 5g,h), supporting the feasibility of generating a clonally diverse, multiplex prime-edited graft that is resistant to SR-1.

To determine whether epitope-edited CD34$^+$ HSPCs could maintain long-term repopulating capacity after SR-1 selection, we performed secondary transplantation (Extended Data Fig. 7a–g). Robust multilineage reconstitution was observed in secondary mice receiving bone marrow from no-conditioning groups, regardless of editing (*KIT*^{D121L} plus *BCL11A*$^{+58}$ or *BCL11A*$^{+58}$). By contrast, among mice receiving bone marrow from SR-1–conditioned primary recipients, only grafts containing *KIT*^{D121L} edited cells generated significant secondary engraftment (Extended Data Fig. 7a,b), which was derived exclusively from mtBFP-marked cells (Extended Data Fig. 7c,d). In non-conditioned cohorts, dual staining using SR-1 and 104D2 revealed mixed monoallelic and biallelic edited cells within the mtBFP-marked myeloid compartment (Extended Data Fig. 7e,f). By contrast, secondary recipients derived from SR-1–conditioned mice showed exclusively *KIT*^{D121L} biallelic-edited progeny (Extended Data Fig. 7e), indicating that only fully edited HSCs were capable of serial repopulation at this dose level, thereby explaining the lower haematopoietic output in secondary recipients. As expected, bone marrow from SR-1-conditioned mice edited only at *BCL11A*$^{+58}$ did not engraft in secondary recipients (fewer than 10^3 cells per mouse), confirming that SR-1 eliminated long-term HSCs lacking *KIT* editing (Extended Data Fig. 7b). These results show that *KIT*^{D121L} enables HSPC engraftment despite stem cells-ablating SR-1 levels, allowing effective replacement of established haematopoiesis without skewing clonal diversity.

Immune selection enhances SCD gene therapy

To validate this strategy in disease-relevant cells, we edited SCD patient-derived CD34$^+$ HSPCs at *BCL11A*$^{+58}$ and/or *BCL11A*$^{+55}$ with either *KIT*^{H378R} base editing or *KIT*^{D121L} prime editing and performed erythroid differentiation with escalating doses of the corresponding KIT mAb (Fab-79D or SR-1; Fig. 5i). To model a low-chimerism post-transplant setting, edited cells were mixed with unedited controls before differentiation. Antibody exposure strongly enriched *KIT* and *BCL11A* edits, reaching 83.6% *KIT*, 76.5% *BCL11A*$^{+58}$ and 84.5% *BCL11A*$^{+55}$ in multiplex base editing and 60.8% *KIT* and 59.75% *BCL11A*$^{+58}$ in multiplex prime editing, compared to 22%, 22.7% and 24.5% for base editing and 4.4 and 7.5% for prime editing without mAb (Fig. 5j). Selection was already evident at low mAb doses, consistent with the essential role of SCF–KIT signalling during erythroid differentiation. High-performance liquid chromatography (HPLC) analysis showed increased HbF and corresponding decreased HbS in antibody-selected *KIT* plus *BCL11A*-edited erythroid progeny (Fig. 5k,l). Collectively, these data show that *KIT* epitope editing enables functional co-selection of therapeutic *BCL11A* edits in SCD HSPCs, resulting in HbF induction and concomitant decrease of HbS above clinically relevant thresholds.

Discussion

Nearly all HSCT protocols rely on genotoxic conditioning. Here we establish KIT epitope editing as a versatile platform to enhance antibody-mediated, non-genotoxic conditioning and enable in vivo co-selection of multiplexed genome edits. Although epitope editing has been used to selectively target haematopoietic malignancies without on-target, off-tumour toxicity[36,47,48], our findings significantly expand this concept to encompass HSCT and gene therapy.

Emerging conditioning strategies based on targeted immunotherapies or mobilizing agents[49] have the potential to reduce systemic genotoxicity and accelerate haematopoietic recovery. Early clinical experience with Fc-silenced KIT mAbs support an acceptable safety profile, despite concerns associated with extra-haematopoietic antigen expression (melanocytes, germ cells and Cajal cells). Briquilimab combined with low-intensity irradiation has shown engraftment without mAb-related toxicities in patients with haemoglobinopathies[40], Fanconi anaemia[30] and low-risk myelodysplastic syndrome[40]. However, briquilimab alone does not fully ablate host HSCs[50] and yields suboptimal engraftment unless transplanted HSPCs have an intrinsic selective advantage[30,51]. Moreover, HSPCs must be infused after plasma mAb levels fall below a defined threshold[30]. ADCs[52], such as the fast-clearing α-amanitin conjugate MGTA-117[26], can improve myeloablation and enable rapid donor engraftment while preserving fertility[53]. However, clinical testing resulted in dose-limiting toxicities, including a fatal event, probably reflecting off-target payload effects in KIT-expressing tissues or non-specific amanitin toxicity.

Epitope editing directly addresses these limitations by unlocking two critical advantages: (1) transplantation can be performed at the peak of host HSPC depletion, when bone marrow niches are maximally available; and (2) continued post-transplant mAb dosing, driving progressive in vivo selection. The former can enhance engraftment and avoid antibody wash-out delay, thereby potentially reducing the window of severe haematopoietic aplasia. The latter enables the administration of extended-interval, low-intensity regimens that yield superior expansion of *KIT*-edited HSPCs while minimizing acute toxicities. Together, these features redefine the therapeutic window for biological conditioning, offering modular and safer alternatives to genotoxic regimens.

Epitope editing is particularly suited to autologous gene therapies, where immunologic barriers are absent and partial chimerism is often sufficient for efficacy. Unlike overexpression of chemoresistance genes, such as *MGMT*[54,55], epitope editing uses minimal, nuclease-free engineering of HSPC antigens by base editing or prime editing, avoiding exogenous alterations of HSC biology and use of chemotherapies. Critically, base editing and prime editing enable efficient multiplexing, allowing combination with therapeutic editing. In our experiments, *KIT* and *BCL11A* were efficiently co-edited in primary HSPCs, endowing their progeny with both HbF induction and mAb resistance. Although

we focused on haemoglobinopathies, many disorders that benefit from partial haematopoietic correction or mixed chimerism, including inborn errors of immunity and bone marrow failure syndromes, may be suitable early clinical indications.

Notably, haematopoietic recovery after anti-KIT selection did not result in clonal expansion or dominance. Loss of unedited cells reflected lack of protection rather than proliferative bias, and these findings were unchanged in secondary transplantation. This indicates that the number of edited long-term HSCs transplanted will be a key determinant of clonal repertoire after selection, emphasizing the importance of efficient HSC collection, editing efficiency, and ex vivo preservation. Unlike innate clonal dominance, where driver mutations confer a permanent growth advantage, immune-based selection imposes a cell-extrinsic, tunable and transient advantage that disappears when antibody dosing stops.

Optimization of mAb schedule and cumulative exposure will be crucial to balance niche clearance with preservation of progenitor pools. Larger immunocompetent models (such as non-human primates) will help to define dosing and the theoretical risk of immune response against neo-epitopes[54]. Clinical translation will also be facilitated by growing experience with HSPC genome editing, including CRISPR–Cas9[56], base-editing[57] and prime-editing platforms. Our genomic analyses indicate that *KIT* epitope editing can be achieved with minimal indels and no detectable off-target substitutions. Additionally, the targeted KIT epitopes are distant from known cancer-associated mutational hotspots; thus, residual indels are likely to be spontaneously counter-selected due to decreased cell fitness. By contrast, *BCL11A* editing was associated with PE3-dependent on-target indels and SpRY-ABE8e off-target deamination. These findings underscore the trade-off between efficiency and genomic integrity when multiplex gene editing is used, and support the importance of further optimization, including PAM-restricted base editing and improved PE2 configurations. Ultimately, the safety of this strategy must be weighed against disease-specific risks and available alternatives. Although gene editing carries residual concerns regarding genomic integrity, genotoxic conditioning remains the dominant source of morbidity in current HSPC therapies. In the BEAM-101 study, a patient died four months after infusion, probably owing to busulfan-related toxicities. Although Cas9 disruption of the *BCL11A* erythroid enhancer was reported to impair erythroid precursor expansion in model systems[58], the most common grade 3–4 adverse events associated with Casgevy are linked to myeloablative conditioning. Finally, the modularity of our approach extends beyond *KIT* and *BCL11A*. Other surface antigen genes could be explored to identify epitope-disrupting mutations paired with diverse therapeutic edits. Epitope editing can also be combined with CAR-T cells, ADCs or bispecific antibodies directed against host haematopoiesis and malignant cells, offering a dual-arm strategy for disease clearance and haematopoietic replacement.

In conclusion, our findings support the paradigm-shifting potential of epitope editing to design next-generation HSCT. By decoupling stem cell conditioning from toxicity, this approach overcomes key obstacles to the broader deployment of gene and cell therapies. Moreover, in vivo co-delivery of therapeutic and epitope edits could leverage immune-mediated selection to enrich genome-modified cells within the host. We envision a future where patients receive life-saving stem cell therapies without risks of prolonged aplasia, infertility or secondary malignancies, and with minimal or no hospitalization.

Online content

Any methods, additional references, Nature Portfolio reporting summaries, source data, extended data, supplementary information, acknowledgements, peer review information; details of author contributions and competing interests; and statements of data and code availability are available at https://doi.org/10.1038/s41586-026-10737-8.

1. Fein, J. A. et al. Early organ toxicity following allogeneic hematopoietic stem cell transplantation differs by conditioning regimen. *Blood* **134**, 4489–4489 (2019).
2. Gyurkocza, B. & Sandmaier, B. M. Conditioning regimens for hematopoietic cell transplantation: one size does not fit all. *Blood* **124**, 344 (2014).
3. Mohty, B. & Mohty, M. Long-term complications and side effects after allogeneic hematopoietic stem cell transplantation: an update. *Blood Cancer J.* **1**, e16–e16 (2011).
4. Hierlmeier, S., Eyrich, M., Wölfl, M., Schlegel, P. G. & Wiegering, V. Early and late complications following hematopoietic stem cell transplantation in pediatric patients – a retrospective analysis over 11 years. *PLoS ONE* **13**, e0204914 (2018).
5. Chhabra, A. et al. Hematopoietic stem cell transplantation in immunocompetent hosts without radiation or chemotherapy. *Sci. Transl. Med.* **8**, 351ra105 (2016).
6. Xue, X. et al. Antibody targeting KIT as pretransplantation conditioning in immunocompetent mice. *Blood* **116**, 5419–5422 (2010).
7. Czechowicz, A., Kraft, D., Weissman, I. L. & Bhattacharya, D. Efficient transplantation via antibody-based clearance of hematopoietic stem cell niches. *Science* **318**, 1296–1299 (2007).
8. Reshetnyak, A. V. et al. Structural basis for KIT receptor tyrosine kinase inhibition by antibodies targeting the D4 membrane-proximal region. *Proc. Natl Acad. Sci. USA* **110**, 17832–17837 (2013).
9. Broudy, V. C. et al. Isolation and characterization of a monoclonal antibody that recognizes the human c-*kit* receptor. *Blood* **79**, 338–346 (1992).
10. Gaudelli, N. M. et al. Programmable base editing of A•T to G•C in genomic DNA without DNA cleavage. *Nature* **551**, 464–471 (2017).
11. Anzalone, A. V. et al. Search-and-replace genome editing without double-strand breaks or donor DNA. *Nature* **576**, 149–157 (2019).
12. Canver, M. C. et al. *BCL11A* enhancer dissection by Cas9-mediated in situ saturating mutagenesis. *Nature* **527**, 192–197 (2015).
13. Bauer, D. E. et al. An erythroid enhancer of *BCL11A* subject to genetic variation determines fetal hemoglobin level. *Science (1979).* **342**, 253–257 (2013).
14. Copelan, E. A. Hematopoietic stem-cell transplantation. *New Engl. J. Med.* **354**, 1813–1826 (2006).
15. Auletta, J. J. et al. Real-world data showing trends and outcomes by race and ethnicity in allogeneic hematopoietic cell transplantation: a report from the Center for International Blood and Marrow Transplant Research. *Transplant. Cell. Ther.* **29**, 346.e1–346.e10 (2023).
16. Ferrari, S. et al. Genetic engineering meets hematopoietic stem cell biology for next-generation gene therapy. *Cell Stem Cell* **30**, 570 (2023).
17. Martin, P. J. et al. Life expectancy in patients surviving more than 5 years after hematopoietic cell transplantation. *J. Clin. Oncol.* **28**, 1011–1016 (2010).
18. Bonifazi, F. et al. Diagnosis and treatment of VOD/SOS after allogeneic hematopoietic stem cell transplantation. *Front. Immunol.* **11**, 489 (2020).
19. Zeiser, R. & Blazar, B. R. Acute graft-versus-host disease — biologic process, prevention, and therapy. *New Engl. J. Med.* **377**, 2167–2179 (2017).
20. Nagler, A. & Shimoni, A. in *The EBMT Handbook* (eds Carreras, E. et al.) 99–107 (Springer, 2019).
21. Vargas-Díez, E., Fernández-Herrera, J., Marin, A., Cámara, R. & García-Díez, A. Analysis of risk factors for acute cutaneous graft-versus-host disease after allogeneic stem cell transplantation. *Br. J. Dermatol.* **148**, 1129–1134 (2003).
22. Chhabra, S. et al. Myeloablative vs reduced-intensity conditioning allogeneic hematopoietic cell transplantation for chronic myeloid leukemia. *Blood Adv.* **2**, 2922–2936 (2018).
23. Czechowicz, A. et al. Selective hematopoietic stem cell ablation using CD117-antibody-drug-conjugates enables safe and effective transplantation with immunity preservation. *Nat. Commun.* **10**, 1526 (2019).
24. Myburgh, R. et al. Anti-human CD117 CAR T-cells efficiently eliminate healthy and malignant CD117-expressing hematopoietic cells. *Leukemia* **34**, 2688–2703 (2020).
25. Arai, Y. et al. Myeloid conditioning with c-kit-targeted CAR-T cells enables donor stem cell engraftment. *Mol. Ther.* **26**, 1181–1197 (2018).
26. Pearse, B. R. et al. A CD117-amanitin antibody drug conjugate (ADC) effectively depletes human and non-human primate hematopoietic stem and progenitor cells (HSPCs): targeted non-genotoxic conditioning for bone marrow transplant. *Biol. Blood Marrow Transplant.* **25**, S29–S30 (2019).
27. Palchaudhuri, R. et al. Non-genotoxic conditioning for hematopoietic stem cell transplantation using a hematopoietic-cell-specific internalizing immunotoxin. *Nat. Biotechnol.* **34**, 738–745 (2016).
28. Srikanthan, M. et al. Non-genotoxic conditioning efficiently depletes host hematopoietic stem cells and facilitates robust multi-lineage engraftment in a mouse model of Fanconi anemia. *Blood* **132**, 2041–2041 (2018).
29. Schiroli, G. et al. Preclinical modeling highlights the therapeutic potential of hematopoietic stem cell gene editing for correction of SCID-X1. *Sci. Transl. Med.* **9**, eaan0820 (2017).
30. Agarwal, R. et al. rradiation- and busulfan-free stem cell transplantation in Fanconi anemia using an anti-CD117 antibody: a phase 1b trial. *Nat. Med.* **31**, 3183–3190 (2025).
31. Jung, D., Long-Boyle, J. R., Pang, W. W. & Gobburu, J. V. S. Pharmacokinetics of briquilimab as a conditioning agent for hematopoietic stem cell transplantation in patients with severe combined immunodeficiency, myelodysplastic syndrome, or acute myeloid leukemia. *Transplant. Cell. Ther.* **30**, 923.e1–923.e9 (2024).
32. Westervelt, P. et al. Mgta-117, an anti-CD117 antibody–drug conjugated with amanitin, in participants with relapsed/refractory adult acute myeloid leukemia (AML) and myelodysplasia with excess blasts (MDS-EB): safety, pharmacokinetics and pharmacodynamics initial findings from a phase 1/2 study. *Blood* **140**, 2117–2119 (2022).
33. Villa, A., Capo, V. & Castiello, M. C. Innovative cell-based therapies and conditioning to cure RAG deficiency. *Front. Immunol.* https://doi.org/10.3389/fimmu.2020.607926 (2020).

34. Andreani, M., Testi, M., Battarra, M. & Lucarelli, G. Split chimerism between nucleated and red blood cells after bone marrow transplantation for haemoglobinopathies. *Chimerism* **2**, 21–22 (2011).
35. Fitzhugh, C. D. et al. At least 20% donor myeloid chimerism is necessary to reverse the sickle phenotype after allogeneic HSCT. *Blood* **130**, 1946–1948 (2017).
36. Casirati, G. et al. Epitope editing enables targeted immunotherapies for acute myeloid leukemia. *Nature* **621**, 404–414 (2023).
37. Locatelli, F. et al. Exagamglogene autotemcel for transfusion-dependent β-thalassemia. *New Engl. J. Med.* **390**, 1663–1676 (2024).
38. Zeng, J. et al. Gene editing without ex vivo culture evades genotoxicity in human hematopoietic stem cells. *Cell Stem Cell* **32**, 191–208.e11 (2025).
39. Gandhi, A. et al. Final results from phase 1 study of briquilimab, an anti-CD117 monoclonal antibody, in combination with low dose irradiation and fludarabine conditioning, shows durable remissions in older adults with acute myeloid leukemia in complete remission and myelodysplastic syndrome undergoing allogeneic hematopoietic cell transplantation. *Blood* **142**, 470 (2023).
40. Hsieh, M. et al. Adding CD117 antibody to alemtuzumab, low dose total body irradiation (TBI), and sirolimus for matched related donor (MRD) hematopoietic cell transplant (HCT) in sickle cell disease (SCD): initial results. *Blood* **144**, 1141–1141 (2024).
41. Yan, J. et al. Improving prime editing with an endogenous small RNA-binding protein. *Nature* **628**, 639–647 (2024).
42. Levesque, S., Cosentino, A., Verma, A., Genovese, P. & Bauer, D. E. Enhancing prime editing in hematopoietic stem and progenitor cells by modulating nucleotide metabolism. *Nat. Biotechnol.* **43**, 534–538 (2024).
43. Tsai, S. Q. et al. GUIDE-seq enables genome-wide profiling of off-target cleavage by CRISPR-Cas nucleases. *Nat. Biotechnol.* **33**, 187–197 (2014).
44. Lazzarotto, C. R. et al. Sensitive and unbiased genome-wide profiling of base-editor-induced off-target activity using CHANGE-seq-BE. *Nat. Biotechnol.* https://doi.org/10.1038/s41587-025-02948-7 (2026).
45. Haeussler, M. et al. Evaluation of off-target and on-target scoring algorithms and integration into the guide RNA selection tool CRISPOR. *Genome Biol.* **17**, 148 (2016).
46. Giannoukos, G. et al. UDiTaS, a genome editing detection method for indels and genome rearrangements. *BMC Genomics* **19**, 212 (2018).
47. Wellhausen, N. et al. Epitope editing in hematopoietic cells enables CD45-directed immune therapy. *Blood* **140**, 862–864 (2022).
48. Garaudé, S. et al. Selective haematological cancer eradication with preserved haematopoiesis. *Nature* **630**, 728–735 (2024).
49. Omer-Javed, A. et al. Mobilization-based chemotherapy-free engraftment of gene-edited human hematopoietic stem cells. *Cell* **185**, 2248–2264.e21 (2022).
50. Kwon, H. S. et al. Anti-human CD117 antibody-mediated bone marrow niche clearance in nonhuman primates and humanized NSG mice. *Blood* **133**, 2104–2108 (2019).
51. Agarwal, R. et al. JSP191 as a single-agent conditioning regimen results in successful engraftment, donor myeloid chimerism, and production of donor derived naïve lymphocytes in patients with severe combined immunodeficiency (SCID). *Blood* **138**, 554–554 (2021).
52. Czechowicz, A. et al. Selective hematopoietic stem cell ablation using CD117-antibody-drug-conjugates enables safe and effective transplantation with immunity preservation. *Nat. Commun.* **10**, 617 (2019).
53. Uchida, N. et al. Fertility-preserving myeloablative conditioning using single-dose CD117 antibody-drug conjugate in a rhesus gene therapy model. *Nat. Commun.* **14**, 6291 (2023).
54. Gori, J. L., Beard, B. C., Ironside, C., Karponi, G. & Kiem, H. P. In vivo selection of autologous MGMT gene-modified cells following reduced-intensity conditioning with BCNU and temozolomide in the dog model. *Cancer Gene Ther.* **19**, 523–529 (2012).
55. Adair, J. E. et al. Extended survival of glioblastoma patients after chemoprotective HSC gene therapy. *Sci. Transl. Med.* **4**, 133ra57 (2012).
56. Frangoul, H. et al. Exagamglogene autotemcel for severe sickle cell disease. *New Engl. J. Med.* **390**, 1649–1662 (2024).
57. Chockalingam, P. S. et al. Impact of BEAM-101 treatment on red blood cell hemoglobin expression, rheology and sickling properties: initial data from the BEACON phase 1/2 study of autologous CD34⁺ base edited hematopoietic stem cells in sickle cell disease. *Blood* **144**, 4957–4957 (2024).
58. Jang, Y. et al. BCL11A-deficient human erythropoiesis is impaired in vitro and after xenotransplantation into mice. *Blood Adv.* **9**, 2722–2732 (2025).

Methods

Sleeping Beauty transgene overexpression

Bidirectional Sleeping Beauty plasmids encoding codon-optimized cDNA of the gene of interest (*KIT*) or its mutated variants were cloned downstream of an EF1α promoter. The same construct included a reporter cassette constituted by a fluorescent protein (mTagBFP2) and puromycin-acetyltransferase (PAC) separated by a P2A peptide downstream of an RPBSA chimeric promoter. dsDNA inserts used for cloning were synthesized by IDT (IDT gBlocks). Human (K562, HEK-293T) or mouse (NIH-3T3 or Ba/F3) cell lines were electroporated using Lonza 4D-Nucleofector system according to the manufacturer's instructions with 500 ng pSB100x transposase plasmid (Addgene #34879) and 100 ng of the transfer plasmid, unless stated otherwise. Cells underwent puromycin selection (1–2 μg ml^{-1}) starting 5 days after electroporation and analysed by flow cytometry 7–14 days after the start of the selection.

KIT mAbs

The SR-1 mAb (mouse IgG2a) was produced by BioXcell. The BA7.3 C.9 hybridoma line was purchased through ATCC and sent to BioXcell for mAb production and purification. SR-1 later became available as BioXcell InVivoMAb anti-human KIT (BE0380). Fab-79D was produced as recombinant mAb by Genescript using the TurboCHO service as human IgG1. A briquilimab research analogue sharing the publicly available sequence of briquilimab (record UNII QWX84D0DRC, DrugBank accession DB18136) was produced as an aglycosylated (N297Q) recombinant mAb by Genescript.

KIT degenerate codon library

We cloned a bidirectional Sleeping Beauty plasmid encoding for a codon-optimized human KIT cDNA bearing unique restriction sites flanking each ECD and a reporter cassette composed of mTagBFP2-P2A-puromycin *N*-acetyl-transferase (PAC). To introduce random amino acids, we generated a library insert by PCR amplification of 350 bp long pooled ssDNA oligos (IDT oPools), encoding the KIT ECD2 bearing degenerate bases (NNN) at each amino acid position, flanked by homology arms for the backbone plasmid. The gel-purified insert was then cloned into the Sleeping Beauty transfer by HiFi cloning (NEB E2621L) and plated on 10× 15 cm agar dishes to estimate library complexity by counting bacterial colonies. Electroporation of HEK-293T cells with low plasmid doses (50–250 ng per 100 μl electroporation volume) allowed to select cells transduced with (~5–10%) efficiency and obtain approximately 1 integration per cell. Sorting of cells positive for KIT control antibody (104D2 clone) and negative for therapeutic SR-1 clone and cells positive for both antibodies was carried out using a BD Melody or BD FACS Aria sorter. Genomic DNA (gDNA) of sorted fractions was extracted (Qiagen DNAeasy Blood&Tissue Kit, 69504) and the library region was amplified by PCR with primers bearing Illumina partial adapters for NGS sequencing (Genewiz Amplicon EZ, Azenta Life Sciences).

Fluorescent ligand binding assay

hSCF (Peprotech 300-07) was resuspended at 1 mg ml^{-1} and conjugated with AlexaFluor-488 or AlexaFluor-647 (Invitrogen AF488 or AF647 Antibody Labeling Kit, A20181 and A20186) for 1 h at room temperature. The reaction was quenched with 1% 1 M Tris-HCl pH 8. Cell lines transduced with the respective KIT variant by Sleeping Beauty transposase were incubated in the presence of AF488-conjugated SCF for 15 min at room temperature, washed with PBS + 2% FBS and analysed by flow cytometry. The data obtained from the antibody and ligand affinity assays at different concentrations were analysed using Graphpad Prism v10.5.

Base editing and prime editing of cell lines

Human K562 cells were cultured in IMDM supplemented with 10% fetal bovine serum (FBS), 1% penicillin-streptomycin (10,000 U ml^{-1}), 2% L-glutamine (200 mM). For base-editing and prime-editing experiments, K562 cells were collected and resuspended in electroporation solution[59] supplemented with 500 ng base editor plasmid and 150-360 pmol of sgRNA (IDT) in a 20 μl electroporation volume. Cells were electroporated using Lonza 4D-Nucleofector system (FF-120 pulse) and cultured for 72 h before evaluation by flow cytometry or gDNA collection.

Base editing and prime editing evaluation by Sanger sequencing

gDNA was extracted using DNeasy Blood & Tissue Kit (Qiagen no. 69506) or QuickExtract solution (Lucigen, QE0905T). PCR amplification of the 350–600 bp region surrounding the target residue was performed using GoTaq G2 polymerase (Promega, M7848) and purified using SV-Wizard PCR Clean-Up kit (Promega, A9282) or sparQ PureMag magnetic beads (QuantaBio, 95196-060). Sanger sequencing was performed through Genewiz (Azenta Life Sciences). Base editing outcomes were estimated using editR v1.08 R package[60] for both base editing and prime editing, as the intended edits accounted for single base substitutions with no indels.

In vitro antibody-mediated selection assays

Human stem cells (mobilized peripheral blood-derived CD34$^+$ HSPCs, either unmodified or edited for KIT) were plated in flat-bottom 96-well plates, with 10,000-15,000 cells per well in StemCell SFEMII medium supplemented with 100 ng ml^{-1} human SCF (Peprotech). SR-1 or Fab-79D anti-KIT mAbs were then diluted to the indicated concentrations in SFEMII medium and then added to the cultured cells, with technical quadruplicates. The plates were incubated at 37 °C in a humidified incubator with 5% CO_2 for 3 days (early time point) or 7 days (late time point). For analysis, cells were transferred to V-bottom plates supplemented with 10–15 μl Countbeads (Biolegend 424902), centrifuged and resuspended in staining mix, containing human Fc-blocking reagent (Miltenyi 130-059-901) and anti-CD34-BV421, CD133-PE, CD90 APC and CD45RA APC-Cy7 mAbs (Biolegend; see Supplementary Table 3). After incubation at room temperature for 15 min, the cells were washed and resuspended in AnnexinV binding buffer (Biolegend 422201) containing AnnexinV FITC or Pacific Blue (Biolegend 640945 or 640918) and 7-AAD. Plates were analysed using a BD Fortessa high-throughput system (HTS) and acquired with BD FACS Diva software v6. Absolute counts of live (AnnV-7-AAD-) target cells were calculated using CountBeads and normalized on the no-antibody condition (absolute count of cells divided by the median of the cells in the no-antibody replicates).

Base editor mRNA in vitro transcription

Base editor or prime editor mRNA was prepared by T7 run-off in vitro transcription (IVT) using a custom plasmid template encoding for a T7 promoter, a minimal 5′ UTR, the base editor reading frame, 2× HBB 3′ UTR and a 110-120-bp poly-A sequence[61]. The plasmid template was linearized by BbsI-HF restriction digestion (NEB, R3539) and purified by phenol-chloroform extraction (Sigma Aldrich, P2069). mRNA IVT was performed using NEB HiScribe T7 kit (E2040S) and co-transcriptionally capped with ARCA (3′-*O*-Me-m7G(5′)ppp(5′)G RNA cap analogue, NEB S1411L) or CleanCap AG (Trilink N-7113). Partial (75%) or total UTP substitution with N1-methyl-pseudo-UTP (Trilink N-1103) or 5-methoxy-UTP (Trilink N-1093) was performed as indicated. DNAse treatment (NEB M0303L) was added after IVT reaction (30 min at 37 °C). IVT mRNA was purified using NEB Monarch RNA Cleanup kit (T2050L) and resuspended in RNase-free water. mRNA was quantified using a Nanodrop-8000 Spectrophotometer and quality control was performed using Agilent Fragment Analyzer with RNA Kit-15NT (Agilent DNF-471). For Vpx mRNA, we used a template containing a 5′ UTR composed of an eIF4G aptamer, a Kozak sequence, the Vpx cassette, and a 3′ UTR constituted by the Woodchuck Hepatitis Virus Post-transcriptional Regulatory Element (WPRE) sequence. This template was prepared by PCR using a forward primer to correct a T7

promoter inactivating mutation and a reverse primer to append a 119-nt poly(A) tail to the 3′ UTR.

CD34$^+$ base editing and prime editing

Cryopreserved human CD34$^+$ HSPCs from mobilized peripheral blood of eight deidentified healthy donors were obtained from the Fred Hutch Cooperative Center of Excellence in Hematology (U54 DK106829). Plerixafor-mobilized peripheral blood from patients with SCD was procured after Boston Children's Hospital institutional review board (IRB) approval and patient-informed consent. CD34$^+$ HSPCs were isolated using the CliniMACS CD34 reagent (Miltenyi, 130-017-501) and CliniMACS LS tubing set (Miltenyi, 170-076-651). CD34$^+$ HSPCs were thawed, cultured, and electroporated as previously described[36]. In brief, cryopreserved cells were thawed in RPMI + 20% FBS and cultured in StemSpan SFEMII medium (StemCell 09655) supplemented with 1% penicillin-streptomycin (10,000 U ml^{-1}), 1% L-glutamine (200 mM), 150 ng ml^{-1} hSCF (Peprotech 300-07), 150 ng ml^{-1} hFLT3L (Peprotech 300-19), 75 ng ml^{-1} hTPO (Peprotech 300-18), 0.75 mM StemRegenin-1 (StemCell 72344), 35 nM UM171 (Sellekchem, S7608), unless stated otherwise. For experiments comparing SFEMII versus X-VIVO15 medium (Lonza 02-060Q) for prime editing, supplements, and concentrations are reported in Extended Data Fig. 4d. Cells were collected and electroporated using Lonza 4D-Nucleofector system 24 h (for prime editing) or 48 h (for base editing) after thawing. Cells were resuspended in P3 solution (Lonza V4XP-3024) supplemented with 60–240 nM base editor or prime editor mRNA, 10–20 μM sgRNA or pegRNA (IDT) and 1.2 U ml^{-1} RNAse inhibitor (Promega RNAsin Plus, N2611). In PE3 experiments, the nicking guide(s) was added at half the concentration of the pegRNA. We used electroporation pulse EO100 or CA-137 for base editing (see Extended Data Fig. 1b), and DS-130 for prime editing (see Extended Data Fig. 4c). For in vivo experiments, cells were counted and transplanted 24 h after the electroporation or, for in vitro experiments, cultured for an additional 5–7 days in the same medium described above at a density of 0.5 million per ml.

In vitro erythroid differentiation

Bone marrow cells collected from humanized mice or cultured CD34$^+$ HSPCs were transferred into erythroid differentiation medium (EDM) consisting of IMDM (GibcoTM, 12440061) supplemented with 330 μg ml^{-1} holo-human transferrin (Sigma, T0665-1G), 10 μg ml^{-1} recombinant human insulin (Sigma, 19278-5 ML), 2 IU ml^{-1} heparin (Sigma, 19278-5 ML), 5% human solvent detergent pooled plasma AB (Rhode Island Blood Center), 3 IU ml^{-1} erythropoietin (Amgen, 55513-144-10). During days 0-7 of culture in EDM-1, EDM was further supplemented with 10-6 M hydrocortisone (Sigma Aldrich, H0135), 100 ng ml^{-1} human SCF (CellGenix, 1418-050) and 5 ng ml^{-1} of recombinant human IL-3 (Peprotech, 200-03). During days 7-11 of culture in EDM-2, EDM was supplemented with 100 ng ml^{-1} human SCF (CellGenix, 1418-050). During days 11-18 of culture in EDM-3, EDM had no additional supplements. Differentiated cells were then used for experimental readouts.

Haemoglobin HPLC

Haemolysates were prepared from erythroid cells after 18 days of erythroid differentiation using Hemolysate reagent (Helena Laboratories 5125) and analysed with D-10 Hemoglobin Analyzer (Bio-Rad) according to the manufacturer's recommendations.

Genotyping and haemoglobin measurement of single-cell-derived erythroid colonies

Single cells derived from human CD34$^+$ HSPCs were FACS-sorted 24 h after editing. The cells were sorted by BCL2-ARIA II SPEC (BD Biosciences) into 150 μl of EDM-1 (see in vitro erythroid differentiation) in 96-well round-bottom plates (ThermoFisher Scientific, 3799) at one cell per well. After 7 days of EDM-1 culture, if colonies were visible at the round bottom of plates, the medium was exchanged to 300 μl of EDM-2. After an additional 4 days of EDM-2 culture, half of the cells were kept in 500 μl of EDM-2, while half of the cells were passaged into 300 μl of EDM-3. After an additional 7 days of EDM-3 culture, cells in EDM-2 were used for genotyping analysis, whereas cells in EDM-3 were used for haemoglobin HPLC measurement.

Fluorescent barcoded library preparation

To generate fluorescently labelled barcoded lentivirus libraries, we cloned a hPGK-mNeonGreen or hPGK-mTagBFP cassette followed by an SV40 polyadenylation signal into a third generation lentivirus backbone in antisense direction. We placed MluI and XbaI unique restriction sites in the 3′ UTR region just downstream of the fluorescent protein stop codon to enable cloning of the barcoded oligo. A 125–127 bp long Ultramer (IDT) with appropriate homology regions and containing 7 stretches of 4 degenerate bases (NNNN, for a total of 28 N), separated by constant anchors, was directly used for cloning through NEB HiFI Assembly. Plating into 15-cm LB-Agar dishes enabled colony screening to ensure product purity and estimation of library complexity, with a minimum goal of 100,000 bacterial colonies. Recovery of the bacteria into liquid LB medium and a short (3 h) growth at 37 °C enabled the extraction of sufficient plasmid material for downstream steps (Macherey-Nagel NucleoBond Xtra Maxi Plus EF 740426.50). Lentiviral production was performed by Calcium-Phosphate transient transfection of the packaging and transfer plasmids (pMDL-RRE, pREV, pMD2, pAdvantage) into HEK-293T cells growing at ~70% confluency. Medium was exchanged 12 h after transfection and, after 30 h since medium change, the culture supernatant was collected, filtered through a 0.22-μm filter and ultracentrifuged at ~72,000*g*, for 2 h at 20 °C using a Beckman Optima L-90K centrifuge to achieve 500× concentration. Viral preps were titrated by serial dilution on HEK-293T cells and transduced cells analysed by flow after 7–14 days to calculate functional titre (TU ml^{-1}). Lentiviral transduction of primary mobilized peripheral blood-derived CD34$^+$ HSPCs was performed after overnight culture (12–24 h after thawing) at multiplicity of infection = 30 in the presence of 8 μM Cyclosporine H (Sigma) as transducer enhancer to achieve >70–80% transduction. In experiments where CD34$^+$ HSPCs are both transduced and base-edited or prime-edited, cells were electroporated 24 h after lentivirus transduction.

In vivo xeno-transplantation experiments

All animal experiments were performed in accordance with regulations set by the American Association for Laboratory Animal Science and Institutional Animal Care and Use Committee (IACUC) approved protocol (DFCI#21-002). Mice were housed in specific pathogen–free facility (temperature 20–24 °C; relative humidity 30–70%) with sterile individually ventilated cages and fed autoclaved food and water, with a standard 12 h day/night light cycle. Six- to eight-week-old female[62] *NOD.Cg-Kit*$^{W\text{-}41J}$ *Tyr*$^+$ *Prkdc*^{scid} *Il2rg*^{tm1Wjl}/ThomJ mice (NBSGW, Jackson Laboratories, 026622) were xeno-transplanted with 1 million human CD34$^+$ HSPCs per mouse by tail vein injection. Human engraftment was monitored by peripheral blood flow analysis at 7–9 weeks. Anti-KIT/CD117 mAbs were administered to NBSGW mice by intravenous or intraperitoneal injection at the indicated intervals and for the indicated number of doses. Unless otherwise specified, doses are reported as absolute mass (mg) per mouse; approximate mg kg^{-1} equivalents were additionally calculated using an average adult female NBSGW body weight of ~25 g (0.025 kg) to facilitate cross-study comparison. Cumulative antibody exposure for each regimen was defined as the sum of all administered doses. Antibodies were diluted in sterile vehicle (PBS) and injected in a constant volume per dose (0.2 ml); control groups received matched vehicle. At the end of the experiment, bone marrow (hind limbs and sternum), spleen, and peripheral blood were collected for FACS and genomic analyses. To evaluate editing efficiency within different haematopoietic subsets, ~20% of total bone marrow cells were FACS-sorted

to isolate haematopoietic lineages ($CD33^+$ myeloid, $CD19^+$ lymphoid, and $CD33^-CD19^-CD34^+$ progenitors), then used for gDNA extraction. Secondary transplantation was performed by transplanting total bone marrow from primary recipients into a second cohort of NBSGW mice. Bone marrow cells were administered intravenously either as freshly prepared single-cell suspensions or after thawing from viable cryopreserved bone marrow samples. Each secondary recipient received ~25% of the total bone marrow cells obtained from a single primary donor mouse. Mice were monitored by peripheral blood analysis to confirm human engraftment and euthanized after 16–18 weeks.

Colony-forming assays

CFU assays were performed by plating 1,000 $CD34^+$ cells per well, for in vitro $CD34^+$ HSPCs experiments, or 25,000 total bone marrow cells per well for xeno-transplanted bone marrow-derived assays, unless stated otherwise. Cells were resuspended in Methocult H4034 medium (StemCell 04034) and plated in SmartDish meniscus-free six-well plates. Wells were imaged and analysed after 2 weeks using StemCell STEMvision system and STEMvision software using the 14-day bone marrow setting. For flow cytometry analysis, methylcellulose medium was softened with pre-warmed PBS, collected, and washed twice before analysis. Myeloid and erythroid cell discrimination was achieved by staining for CD33 and CD71, respectively, while mNG and mtBFP detection enabled the identification of the edited versus non-edited cell of origin.

Myeloid differentiation culture and phosphoflow analysis of HSPCs

$CD34^+$ HSPCs derived from three different healthy donors were thawed, cultured in HSC expansion medium and edited as previously described. Five days after electroporation, cells were transitioned to myeloid differentiation medium (SFEMII, penicillin-streptomycin 1%, Q 1%, SCF 100 ng ml^{-1}, FLT3L 100 ng ml^{-1}, TPO 50 ng ml^{-1}, GM-CSF 100 n l^{-1}, IL-6 50 ng ml^{-1}, and IL-3 10 ng ml^{-1} (Peprotech)). After 5 days, cells were starved overnight in SFEMII (not supplemented with cytokines) and then stimulated with SCF 100 ng ml^{-1}, G-CSF 100 ng ml^{-1}, IFNβ 5,000 U ml^{-1}, IFNγ 10 ng ml^{-1}, IL-4 50 ng ml^{-1}, PMA 100 ng ml^{-1} plus Ionomycin 1 μg ml^{-1} or LPS 100 ng ml^{-1} for 20 min at 37 °C. Cells were then collected and immediately fixed with Biolegend fixation buffer (420801) and permeabilized with Biolegend TruePhos Perm Buffer (425401) according to the manufacturer's instructions. Cells were then aliquoted into two fractions and stained with the following antibody mixes: (1) pSTAT1 PE-Cy7, pSTAT3 BV421, pSTAT5 PE, pSTAT6 AF647 and pAKT AF488; (2) pERK1/2 BV421, pMEK1 AF647, p38/MAPK PE and pRPS6 PE-Cy7 (Biolegend). Cells were then analysed on a BD Fortessa Analyzer with HTS sampler.

Gene expression analysis of edited $CD34^+$ HSPCs

RNA-seq gene expression analysis was performed using Plasmidsaurus Nanopore RNA-seq platform. $n = 32$ samples from $CD34^+$ cells isolated from three donors (donors 1, 2 and 3), corresponding to combinations of editing locus (*BCL11A*, *KIT* or *AAVS1*), prime editing strategy (PE2 and/or PE3), and SCF stimulation conditions (unstimulated versus stimulated) were sequenced. Raw fastq files underwent quality assessment using FastQC v0.12.1, followed by quality filtering with fastp v0.24.0 (poly-X tail trimming, 3′ quality-based tail trimming, minimum Phred score of 15, minimum length 50 bp). Quality-filtered reads were aligned to the human reference genome hg38 using STAR v2.7.11 with non-canonical splice junction removal and unmapped read output, followed by coordinates sorting with samtools v1.22.1. PCR and optical duplicates were removed using unique molecular identifier (UMI)-based deduplication (UMIcollapse v1.1.0). Alignment quality, strand specificity, and read distribution were evaluated using RSeQC v5.0.4 and Qualimap v2.3, aggregated into a MultiQC v1.32 report. Gene-level quantification was performed using featureCounts (subread v2.1.1) with strand-specific counting, multi-mapping fractional assignment, and grouping by gene_id. Differential expression analysis was performed in Python using the PyDESeq2 (Love et al., 2014, adapted for Python) implementation of the DESeq2 negative binomial model. Gene-level counts for all retained genes were modelled with the following design formula for the full model:

$$\text{GeneExpr} = \beta_0 + \beta_{\text{donor}} + \beta_{\text{stimulation}} + \beta_{\text{guide}} + \beta_{\text{prime-editor}}$$

with reference levels set to donor-unspecified, unstimulated (unstim), *AAVS1* guide and PE2 prime editor. In this model, β_0 represents the gene-specific intercept corresponding to the reference condition, while β_{donor}, $\beta_{\text{stimulation}}$, β_{guide} and $\beta_{\text{prime-editor}}$ represent gene-specific coefficients for donor, stimulation status, guide/editing locus and prime-editing system, respectively. Donor, guide and prime-editor terms were treated as categorical covariates using reference-level coding. The stimulation coefficient $\beta_{\text{stimulation}}$ was used to test the adjusted main effect of SCF stimulation across donors, guides and prime-editing systems. Model coefficients were tested using the Wald test with Benjamini–Hochberg correction for false discovery rate (FDR) correction. The primary contrast tested was the main effect of stimulation (stimulated versus unstimulated) across all donors, guides, and editing systems, representing the global stimulus response while controlling donor, guide, and prime editing effects. Significant genes were identified using thresholds of adjusted P value < 0.001 with $|\log_2 \text{fold change}| > 1.0$ (moderate). Heat maps of z-score normalized expression for high-confidence differentially expressed genes (adjusted $P < 0.05$, $|\log_2 FC| > 1.5$) were generated using hierarchical clustering (Euclidean distance, Ward linkage) with sample annotations for stimulation, guide, prime editing, and donor, visualized using seaborn clustermap. Figures were generated using matplotlib, seaborn.

Flow cytometry

Cell lines were collected, washed in PBS + 2% FBS, resuspended in 100 ml, incubated with human or mouse Fc-blocking reagent (Miltenyi 130-059-901 and 130-092-575) and then stained with the indicated antibodies for 20-30 min at 4 °C and washed. Viability was assessed by LiveDead yellow (Invitrogen L34959), 7-AAD (Biolegend 420404), or propidium iodide (PI, Biolegend, 421301) staining. Immunophenotyping of in vitro base-edited $CD34^+$ HSPCs was evaluated by staining for 30 min at 4 °C with CD34 BV421, CD45RA APC-Cy7, CD90 APC, and CD133 PE antibodies after incubation with Fc-blocking reagent (Miltenyi 130-059-901). Viability was assessed by 7-AAD or propidium iodide (PI) staining. Peripheral blood collected from in vivo experiments was lysed twice for 10 min at room temperature twice using ACK reagent (StemCell 07850), washed, incubated with human and mouse Fc-blocking reagent (Miltenyi 130-059-901 and 130-092-575) and stained at room temperature for 15 min with hCD45 BV421 or BV786, mCD45 PE, CD3 AF647, CD19 BV605, CD33 PE-Cy7 antibodies, unless stated otherwise. 7-AAD was included as viability stain. To comprehensively identify haematopoietic populations in bone marrow samples[63], collected cells were lysed using ACK reagent, washed twice and supplemented with CountBeads (50–100 μl per tube) for absolute cell number quantification. Samples were then incubated with human and mouse Fc-blocking reagent and stained for 30 min on ice with hCD45 BV786, mCD45 PerCP-Cy5.5, CD3 PE-Cy5, CD7 AF700, CD10 BUV737, CD11c BUV661, CD14 BV510, CD19 BV605, CD33 PE-Cy7, CD38 BUV396, CD45RA APC-Cy7, CD34 BUV496, CD90 APC, FLT3 PE and KIT 104D2 BV711 antibodies (Supplementary Table 3), with the addition of 50 ml per sample Brilliant Stain buffer (BD 659611). In some experiments, a KIT dual staining with SR-1 AF488 and 104D2 BV711 was performed to directly visualize editing status. Cells were acquired on a five-laser BD Fortessa flow cytometer using BD FACS Diva software v6 and analysed using FCS Express 7 (DeNovo Software).

Bioinformatic processing of epitope mapping libraries

Amplicon sequencing data were first processed to merge raw paired-end reads into single consensus sequences using BBMerge, which corrects discrepancies between forward (R1) and reverse (R2) reads. The merged reads were aligned to a DNA reference corresponding to the section of wild-type (WT) KIT sequence undergoing screening using the BWA-MEM algorithm. Only high-confidence alignments were retained by filtering for a mapping quality score (MAPQ) greater than 60, and unmapped or low-quality reads were discarded. High-quality mapped reads were translated into amino acid sequences using the Biopython library. These translated sequences were then compared to the wild-type KIT protein (120 amino acids in length) using BLASTP. The BLASTP output was generated in tabular format (outfmt 6) to report alignment features including query ID, sequence length, per cent identity, number of mismatches, and aligned regions for both query and subject sequences. For each query, the best alignment was selected based on alignment length. Only sequences with an alignment length greater than 110 amino acids were retained to allow flexibility at the read extremities while ensuring coverage of the epitope region. Input sequences containing amino acid insertions relative to the reference were excluded from further analysis. From the filtered BLASTP results, we generated a data matrix for each sample with 22 rows representing the 20 canonical amino acids, the stop codon, and deletions, and 120 columns corresponding to each position in the wild type sequence. Each cell in the matrix records the number of reads in which a given amino acid was observed at a specific position, allowing quantitative profiling of epitope mutation frequency across the entire sequence. The frequency matrices corresponding to single-positive samples (characterized by abrogated binding affinity to the SR-1 antibody) and double-positive samples (with conserved SR-1 binding) were modelled using logistic regression for count data. Specifically, the number of reads carrying a specific mutation over the total number of reads in a sample was modelled to estimate whether significant enrichment of particular mutations was observed in single-positive samples. Statistical significance was assessed using a likelihood ratio test comparing two nested models. As a measure of enrichment or depletion, we used the chi-squared test statistic. A positive value indicates that a mutation is enriched in single-positive samples relative to double-positive samples, while a negative value indicates depletion. P-values associated with mutation enrichment were adjusted for multiple testing using the FDR, and mutations with FDR-adjusted *P* values below 0.05 were considered statistically significant.

Barcode-based clonal tracking of edited HSPCs

To evaluate the clonal architecture of edited haematopoietic populations, barcode libraries were amplified from gDNA extracted from sorted bone marrow fractions, including $CD33^+$ myeloid, $CD19^+$ lymphoid and Lin^-CD34^+ progenitor cells. Libraries were generated using a two-step PCR strategy. In PCR1, library-specific primers targeting the mNG or mtBFP constructs were used to amplify barcode-containing regions (Supplementary Table 2). The forward primer contained a seven-nucleotide degenerate sequence, which served as a UMI to account for PCR amplification bias and enable identification of PCR duplicates. In PCR2, common primers incorporating partial Illumina adapter sequences were used to generate sequencing-ready libraries (Supplementary Table 2). Following amplification, purified PCR products derived from the mNG and mtBFP libraries were pooled for Illumina amplicon sequencing (Amplicon EZ, Azenta). Sequencing reads were first quality filtered using Flexbar (v3.5.0) with a minimum quality threshold of qt = 30, using parameters q = TAIL and qf = i1.8. Only reads passing these criteria were retained for downstream analysis. High-quality reads were processed to detect and annotate the 7-nt UMI embedded in the forward primer using Flexbar (-at LEFT --adapter-trimmed-out ONLY -m 1). UMIs were used for PCR duplicate removal, and the maximum permissible error rate for UMI detection was set to 0.1. A 6-nt unique sequence embedded in the library design was used to assign fluorescence identity (mNG or mtBFP) to each read. Reads were further processed to identify the 28-nucleotide lineage barcode, corresponding to the designed barcode structure NNNNT GNNNNCANNNNACNNNNGANNNNGTANNNNAGCNNNN. Only reads with consistent fluorescence assignments and valid UMI or barcode annotation were retained and exported as text files for downstream processing using custom Python scripts. To reduce artificial inflation of barcode counts arising from sequencing or PCR artefacts, barcode sequences were clustered using the DBSCAN (density-based spatial clustering of applications with noise) algorithm, using Levenshtein distance as a similarity metric with a distance threshold of eight nucleotides (Extended Data Fig. 2j and Supplementary Fig. 1). This approach groups highly similar barcode sequences into unified clusters representing the same clonal lineage, improving the robustness of clonal assignments. Additionally, singleton UMIs (UMIs supported by a single read) were removed to reduce the impact of residual sequencing noise. Clone size was estimated using both total read counts and the number of distinct UMIs associated with each barcode. From these values, clonal diversity metrics were calculated, including species richness (*S*), the Shannon diversity index (*H*), Simpson's diversity index (Simp), and Pielou's evenness index (*J*), enabling quantitative characterization of clonal composition and distribution within each sample.

CHANGE-seq

CHANGE-seq was performed for prime-editing targets as previously described[64]. In brief, the purified gDNA tagmented using custom Tn5-transposome to an average length of 400–800 bp, and gap repaired with HiFi HotStart Uracil+ Ready Mix (Kapa Biosystems KR0413). USER enzyme (NEB M5505L) and T4 polynucleotide was then used to treat the gap-repaired DNA. DNA circularization was performed using T4 DNA ligase (NEB M0202L) and residual traces of linear DNA were removed by exonuclease cocktail and followed by dephosphorylation with Quick CIP (NEB M0525L). In vitro cleavage reactions were performed with 125 ng of circularized DNA, 90 nM SpCas9 protein (NEB), NEB buffer 3.1 (NEB), and 270 nM gRNAs in a 50 µl volume. Cleaved products were incubated with proteinase K (NEB), A-tailed, hairpin adapter (NEB) ligated, and treated with USER enzyme. Products were amplified by PCR with the Kapa HiFi polymerase (Kapa Biosystems), and libraries were quantified by qPCR (Kapa Biosystems) and sequenced on the Illumina NextSeq 2000 with the following cycles 151-8-8-151. CHANGE-seq data analyses were performed using open-source software https://github.com/tsailabSJ/changeseq. Plots representing top nominated sites for each gRNA are reported as Supplementary Figs. 2–5.

CHANGE-seq-BE

CHANGE-seq-BE was performed as previously reported[44] using the same circularized, exonuclease cocktail, and CIP treated gDNA as mentioned above from CHANGE-seq. In brief, ABE in vitro deamination performed in a 50-µl reaction with deamination buffer (50 mM Tris-HCl pH 8.0, 25 mM KCl, 2.5 mM MgSO4, 0.1 mM EDTA, 10% glycerol, 2 mM DTT and 10 µM ZnCl2). ABE and gRNAs final concentrations were 300 nM and 900 nM with 125 ng of circularized DNA. ABE8e-deaminated DNA products were treated with proteinase K (NEB), followed by Endonuclease V (NEB, M0305S) treatment. Linearized DNA fragments were treated with Klenow fragment (3′→5′ exo-, NEB M0212L), dA-tailed, ligated with a hairpin adaptor (NEB), USER treated and amplified by PCR using HiFi HotStart Uracil (Kapa/Roche). Completed libraries were quantified by qPCR using the Kapa library quantification kit and sequenced with 151-bp paired-end reads on an Illumina NextSeq 2000. CHANGE-seq-BE data analyses were performed using open-source software https://github.com/tsailabSJ/changeseq/tree/BE. Plots representing top nominated sites for each gRNA are reported as Supplementary Figs. 2–5.

rhAmpSeq and analysis of off-target base editing and prime editing

Multiplex targeted sequencing (rhAmpSeq, IDT) performed on gDNA extracted from base- or prime- edited CD34$^+$ cells and unedited controls to validate off-target activity from CRISPOR[65], CHANGE-seq, and CHANGE-seq-BE designated sites. Libraries prepared and sequenced with 151-bp paired-end reads on an Illumina NextSeq 2000 according to the manufacturer's protocol. Data was analysed using CRISPResso Pooled (v2.0.41). For base-editing analysis, the parameters were --quantification_window_size 10 --quantification_window_center -10. The percentage of reads containing A-to-G mutations within the protospacer positions 1–10 at on- or off-target sites was used for statistical analysis[44]. For prime editing analysis, the parameters were --quantification_window_size 1 --quantification_window_center -3. For pegRNA off-target analysis, the percentage of substitution that could be encoded by the RTT sequence and the percentage of indels at on- or off-target sites were used for statistical analysis. For nicking sgRNA off-target analysis, only the percentage of indels was used[66]. For the statistical analysis, chi-squared test was performed and false discovery rate (FDR) calculation using the Benjamini–Hochberg method. The reported off-target sites with difference ≥ 0.5% for at least one treatment and with FDR ≤ 0.05 were determined as significant. Custom code was used to conduct base-editing off-target quantification is available from GitHub https://github.com/tsailabSJ/MKSR_off_targets and https://github.com/YichaoOU/PE_off_target.

Uni-directional targeted sequencing

A custom Tn5-transposome with the full-length Illumina forward (i5) adapter, a sample barcode, and unique molecule identifier was used for the gDNA tagmentation. After tagmentation of the gDNA to approximately 1,500 bp fragments, 2 rounds of PCR were performed. The first PCR amplified the target site using the gene-specific anchor primer, and the second round of PCR added the reverse (i7) Illumina adapter with an additional sample barcode. Sequences of oligos and PCR components are provided in Supplementary Table 10. Both PCR1 and PCR2 conditions were as follows: denaturation, 95 °C for 5 min; touchdown (15× cycles), 95 °C, 70 °C, 72 °C for 0.5 min, 2:00 (1 °C per cycle), 0.5 min; amplification (12× cycles), 95 °C, 55 °C, 72 °C for 0.5 min, 1:00, 0.5 min (at 1.2 °C s^{-1} ramp rate); extension 72 °C for 5 min; hold 4 °C. Final libraries were then quantified by qPCR, pooled, and size-selected for 400–850 bp using Yourgene Health LightBench, and then sequenced on an Illumina NextSeq 2000 with 301-8-18-301 cycles. Analysis was performed as previously reported[67]. Source code available at https://github.com/editasmedicine/uditas. UDiTaS was run with parameters -window_size 10 -min_MAPQ 10.

Qualitative junction PCR and ddPCR quantification of prime editing-induced translocations

To detect potential inter-chromosomal rearrangements between the *KIT* and *BCL11A* sites, a panel of cross-chromosomal PCR primer pairs was designed to flank the edited regions of both loci (Supplementary Table 2). The positive strand was defined as the strand with the 5′ end at the short (p) arm terminus, and primers were designated as forward or reverse according to each gene's open reading frame orientation. Two amplicon sizes were evaluated (~400 bp, ~900 bp) to enable orientation-specific detection of reciprocal and non-reciprocal junctions. Primer performance was validated on-target (Promega GoTaq G2 MasterMix), with short amplicons demonstrating superior amplification efficiency and specificity on both loci. We used K562 edited with SpCas9 nuclease and different combinations of KIT and BCL11A pegRNAs and nicking gRNAs to generate positive controls for chromosomal translocations. Annealing temperature for all primer combinations was optimized within the range identified for on-target amplicons (60–67 °C), and 65 °C was selected based on specificity versus unedited controls. Thermal cycling was performed as follows: initial denaturation at 95 °C for 2 min; 35 cycles of 95 °C for 30 s, 65 °C for 30 s, and 72 °C for 45 s; followed by a final extension at 72 °C for 5 min. Amplification products were resolved by agarose gel electrophoresis (1.5–2% agarose in TAE buffer) and visualized by SYBR-based staining. To enable absolute quantification of translocation frequency, ddPCR assays targeting KIT–BCL11A junctions were developed. FAM-fluorescent probes (IDT) were designed for each short-amplicon primer pair (Supplementary Table 2) and tested for on-target and cross-chromosomal amplicon detection, using both gDNA from nuclease-treated cells and spike-in of the gel-purified translocation products generated in the PCR optimization described above. A genomic control locus (TTC5 gene) was used as normalizer (with HEX as fluorophore). ddPCR reactions were prepared according to the manufacturer's recommendations (Bio-Rad QX200 ddPCR system) using ddPCR Supermix no dUTP for probes (Bio-Rad) using 50 ng input gDNA per reaction, with 4 replicate wells per sample (200 ng total input) to maximize assay sensitivity. Thermal cycling was performed for 40 cycles as follows: 95 °C for 3 min; 95 °C for 30 s, 59 °C for 30 s (ramp rate 2 °C s^{-1}), and 72 °C for 1 min; followed by a final extension at 72 °C for 5 min and a 4 °C hold. Droplets were generated using the QX200 Droplet Generator (Bio-Rad) according to the manufacturer's instructions. Data were analysed with QuantaSoft Manager software (Bio-Rad). Positive and negative droplet thresholds were defined based on no-template and unedited genomic controls. Translocation frequencies were calculated as copy number normalized to reference gene copies (n = 2) and reported as events per 1,000 diploid genomes.

Statistical analyses

The n indicates the number of biologically independent samples, animals, or experiments. Data are summarized as mean ± s.d. Inferential techniques were applied in presence of adequate sample sizes ($n \geq 5$), otherwise only descriptive statistics are reported. Comparisons between two groups are performed by unpaired t-test. FDR-adjusted P values are reported when appropriate. When one variable is compared among more than two groups, one-way ANOVA is used. When multiple variables are compared among more than two groups, two-way ANOVA is used. The P value of the row or column effect is reported as appropriate to describe the significance of the selected parameter on the measured variable. Multiple comparisons between groups are performed with two-stage step-up procedure of Benjamini, Krieger and Yekutieli to control the false discovery rate (FDR, Q = 0.05), when appropriate. When dose–response relationships were compared across experimental groups, data were fit by global nonlinear regression using a four-parameter logistic (Hill) model. Differences in HillSlope were evaluated by comparing a constrained model with a shared HillSlope to an unconstrained model allowing group-specific HillSlope values using an extra sum-of-squares F-test (nested model comparison; α = 0.05). In all the analyses, the significance threshold was set at 0.05, and 'NS' means not significant. Data were collected in Microsoft Excel, and statistical analyses were performed in GraphPad Prism v10.5 (GraphPad).

Reporting summary

Further information on research design is available in the Nature Portfolio Reporting Summary linked to this article.

Data availability

All relevant data are included in the manuscript. Source data are provided with this paper.

Code availability

Code used to analyse CHANGE-seq data can be found at https://github.com/tsailabSJ/changeseq. Code used to analyse CHANGE-seq-BE

datasets can be found at https://github.com/tsailabSJ/changeseq/tree/BE. The custom code used to conduct base-editing off-target quantification in rhAmpseq datasets is available at https://github.com/tsailabSJ/MKSR_off_targets and https://github.com/YichaoOU/PE_off_target. The source code to analyse UDiTaS assays is available at https://github.com/editasmedicine/uditas. Sequencing data were aligned to the human reference genome GRCh38 (hg38; Genome Reference Consortium; https://www.ncbi.nlm.nih.gov/datasets/genome/GCF_000001405.40/).

59. Bak, R. O., Dever, D. P. & Porteus, M. H. CRISPR/Cas9 genome editing in human hematopoietic stem cells. *Nat. Protoc.* **13**, 358–376 (2018).
60. Kluesner, M. G. et al. EditR: a method to quantify base editing from Sanger sequencing. *CRISPR J.* **1**, 239–250 (2018).
61. Zeng, J., Casirati, G., Nguyen, M. A., Genovese, P. & Bauer, D. E. Base editing of human hematopoietic stem cells. *Methods Mol. Biol.* **2606**, 43–62 (2023).
62. Notta, F., Doulatov, S. & Dick, J. E. Engraftment of human hematopoietic stem cells is more efficient in female NOD/SCID/IL-2Rgc-null recipients. *Blood* **115**, 3704–3707 (2010).
63. Basso-Ricci, L. et al. Multiparametric whole blood dissection: a one-shot comprehensive picture of the human hematopoietic system. *Cytometry* **91**, 952 (2017).
64. Lazzarotto, C. R. et al. CHANGE-seq reveals genetic and epigenetic effects on CRISPR-Cas9 genome-wide activity. *Nat. Biotechnol.* **38**, 1317–1327 (2020).
65. Concordet, J. P. & Haeussler, M. CRISPOR: intuitive guide selection for CRISPR/Cas9 genome editing experiments and screens. *Nucleic Acids Res.* **46**, W242–W245 (2018).
66. Everette, K. A. et al. Ex vivo prime editing of patient haematopoietic stem cells rescues sickle-cell disease phenotypes after engraftment in mice. *Nat. Biomed. Eng.* **7**, 616–628 (2023).
67. Katta, V. et al. Development and IND-enabling studies of a novel Cas9 genome-edited autologous CD34$^+$ cell therapy to induce fetal hemoglobin for sickle cell disease. *Mol. Ther.* **32**, 3433–3452 (2024).

Acknowledgements We thank all members of the Genovese laboratory for discussion; and B. Besemer, J. P. Gerhards, S. Garg, A. Brandauer and G. Zambonini (Genovese laboratory) for help with some experiments. A.C. conducted this study as partial fulfillment of his Ph.D in Translational and Molecular Medicine, DIMET, Milano-Bicocca University (Italy).

Author contributions G.C. designed and performed research, analysed and interpreted data, and wrote the manuscript. A.C. designed and performed research, and interpreted data. M.F., A. Mucci, M.S.M., E.D., V.C. and F.R. performed experiments. S.L. helped with prime editing experiments. J.Z., S.L. and N.N. optimized *BCL11A* editing and performed erythroid differentiation experiments. J.P.M. provided plerixafor-mobilized SCD HSPCs. V.K., A. Matsubara and Y.L. performed and analysed off-target analyses (CHANGE-seq, CHANGE-seq-BE, UDiTaS and rhAmpseq) under the supervision of S.T. D.P. and M.C.-N. performed bioinformatic analyses of clonal tracking, RNA-seq and epitope mapping from NGS data and provided oversight of statistical analyses. C.B. provided discussion. D.B. supervised research on *BCL11A* editing and provided discussion. P.G. designed research, interpreted data, wrote the manuscript and coordinated the work.

Funding This work was supported by grants to P.G. from the National Institute of Health (R01AI155796, R01HL170629, R01CA286036), the Leukemia Lymphoma Society (TRP 6669-24), the Department of Defense (HT94252411064), the Alex Lemonade's Stand Foundation (Research Catalyst 1266935) and CURE Childhood Cancer (Translation to CURE 1070087); to D.B. from Doris Duke Foundation (2022092), the St. Jude Children's Research Hospital Collaborative Research Consortium, NIH (R01HL170629) and DoD (HT94252411064); and to G.C. from the American Society of Transplantation and Cellular Therapy (ASTCT, New Investigator Award), DKMS John Hansen Research Grant, the American Society for Gene and Cell Therapy (ASGCT) Career Development Award and the PTCTC Jeff Gordon Children's Foundation New Investigator Award. A.C. was partially supported by a fellowship from the American Italian Cancer Foundation (AICF). S.L. holds a Banting Postdoctoral Fellowship from the Canadian Institutes of Health Research (CIHR). E.D. was partially supported by an Innovation Fellowship from the Clinical Immunology Society (CIS) and the Jeffrey Modell Foundation, and the Fondo Italiano per la Scienza (FISO0002235). F.R. was partially supported by a fellowship from the Italian Leukemia Association (AIL) sez. Pavia, a fellowship by Fondazione Enrico ed Enrica Sovena, and a Fondazione Gianni Bonadonna Fellowship, in collaboration with the European School of Oncology. CD34$^+$ cells were provided by the Fred Hutch Cooperative Center of Excellence in Hematology (U54 DK106829).

Competing interests G.C., A.C. and P.G. are inventors of patent applications related to this work (WO2023159136A2 and WO2024148235A1), which are owned and managed by the Boston Children's Hospital and Dana-Farber Cancer Institute. The other authors declare no competing interests.

Additional information

Supplementary information The online version contains supplementary material available at https://doi.org/10.1038/s41586-026-10737-8.

Correspondence and requests for materials should be addressed to Pietro Genovese.

Peer review information *Nature* thanks Hans-Peter Kiem, Vivien Sheehan, who co-reviewed with Sammi Kim, and the other, anonymous, reviewers for their contribution to the peer review of this work. Peer reviewer reports are available.

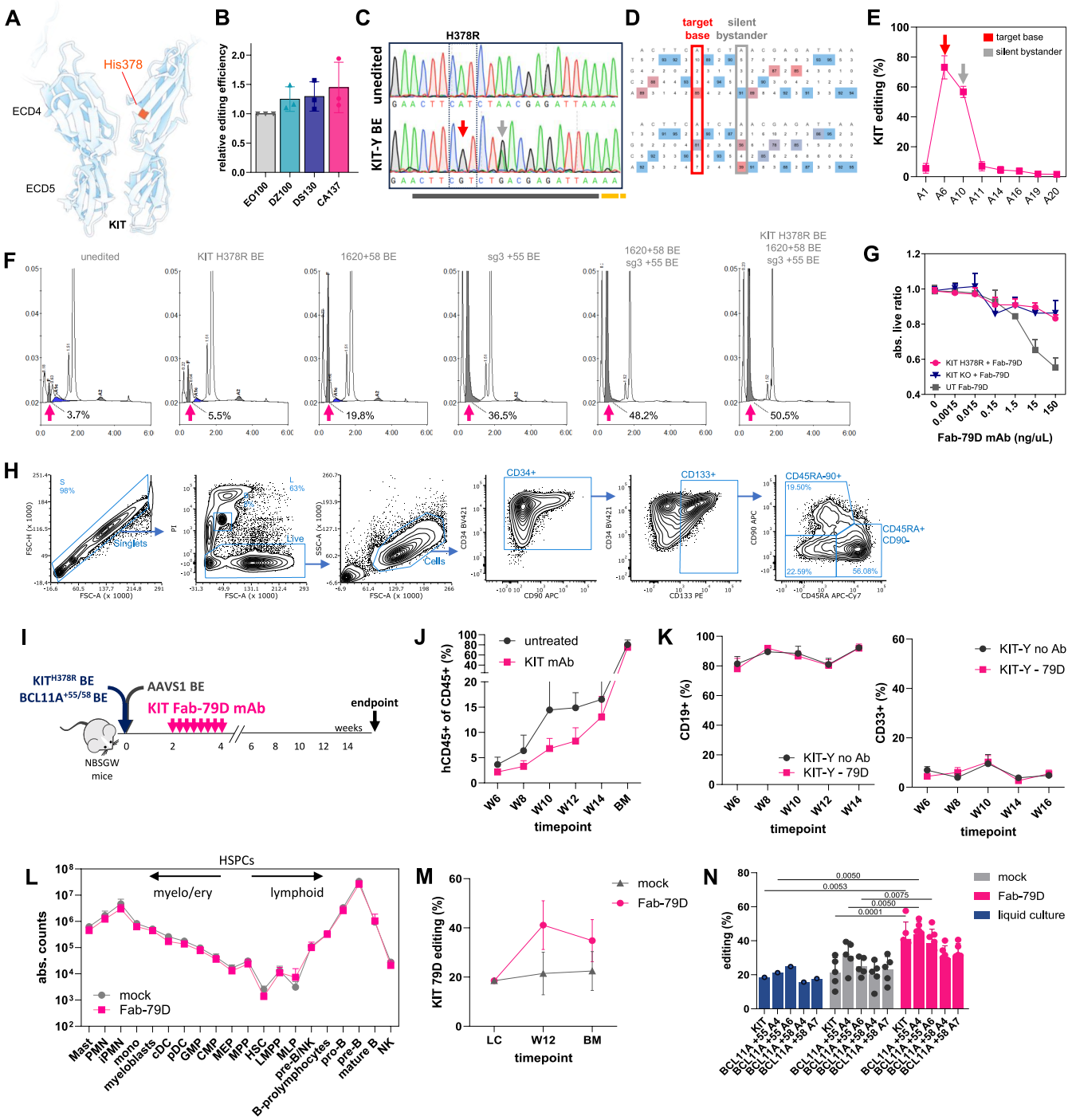

Extended Data Fig. 1 | See next page for caption.

Extended Data Fig. 1 | Functional characterization of KIT^{H378R} and BCL11A$^{+55/+58}$ base edited HSPCs and proof-of-concept in vivo selection. (**A**) Cartoon model of human KIT extracellular domains (ECD4–ECD5). The position of H378 – the residue that is mutated to R to abrogate Fab-79D binding within ECD4 – is highlighted in red. Adapted from https://www.rcsb.org. ref. 2E9W. (**B**) Electroporation pulse optimization for efficient delivery of SpRY-ABE8e mRNA into CD34+ HSPCs using Lonza-4D Nucleofector. Reported editing efficiency is normalized on EO100, which is the pulse recommended by the manufacturer for human CD34+ HSPCs. Mean ± SD. N = 3 experimental replicates. (**C**) Sanger sequencing chromatograms showing efficient adenine base editing (ABE) at the H378 codon (CAT>CGT, red arrow) within KIT ECD4 following ABE (bottom trace). A silent bystander mutation edit is indicated by the grey arrow. The gRNA spacer and the PAM are highlighted by the dark grey and yellow bars at the bottom, respectively. (**D**) Quad-plot indicating the base changes at each position within the KIT-Y sgRNA for editing the H378 codon, with highlighted editing of the target base (red arrow) and the silent bystander adenine (grey arrow). (**E**) Editing efficiency of the As within editing window for KIT-Y sgRNA using SpRY-ABE8e. Target A6 indicated by red arrow, bystander by the grey arrow. Mean ± SD. N = 4 replicates. (**F**) Representative high-performance liquid chromatography (HPLC) plots showing hemoglobin expression profiles in unedited HSPCs, and cells edited with KIT^{H378R} only, BCL11A^{+58} only, BCL11A^{+55} only, BCL11A$^{+58/+55}$ or KIT^{H378R} + BCL11A$^{+58/+55}$. The pink arrow identifies the fetal hemoglobin (HbF) peak along with its relative abundance (%). (**G**) In vitro expansion culture assay of KIT^{H378R} BE, KIT knock-out (KO) and unedited HSPCs, cultured with SCF and with increasing concentrations of Fab-79D antibody. The plot reports absolute counts normalized on no-Ab control to highlight only the effects of Fab-79D-mediated blockade of KIT signaling. KIT^{H378R} BE cells display resistance to SCF-blockade and overlap with KIT^{KO} cells. Mean ± SD. N = 3 replicates. (**H**) Representative flow plots demonstrate the gating strategy for phenotypic characterization of human CD34^{+} HSPCs in liquid culture expansion experiments using CD34, CD133, CD45RA and CD90. (**I**) Schematic of the in vivo competitive transplant experiment performed by mixing KIT and BCL11A edited with *AAVS1* control-edited HSPCs (1:1 ratio) to obtain *proof-of-concept* of the selection of KIT^{H378R} epitope edited HSPCs and their progeny by Fab-79D mAb. BE, base editing. Mock group, N = 5 mice; Fab-79D mAb, N = 7 mice. (**J-K**) Longitudinal analyses of PB by flow cytometry, reporting (**J**), the human engraftment (hCD45+ within total CD45+) and (**K**), the fraction of lymphoid (CD19+, left) and myeloid (CD33+, right) cells within CD45+ human cells. Mean ± SD. N = 5 mice for the untreated group, N = 7 mice for Fab-79D-treated group. (**L**) Absolute counts of hematopoietic lineages in the BM at endpoint by flow cytometry, according to treatment condition. Mean ± SD. N = 5 mice for the untreated group, N = 7 mice for Fab-79D-treated group. (**M**) KIT^{H378R} editing efficiency in the pre-transplant liquid culture (LC), 12-week peripheral blood (W12) and BM at endpoint, according to treatment group. Mean ± SD. N = 5 mice for the untreated group, N = 7 mice for Fab-79D-treated group. (**N**) Editing efficiency of KIT^{H378R} and BCL11A$^{+58/+55}$ loci in pre-transplant liquid culture (LC, blue bars) and BM at endpoint according to treatment group (grey, mock-treated; purple, Fab-79D). Mean ± SD. N = 5 mice for the untreated group, N = 7 mice for Fab-79D-treated group. One-way ANOVA.

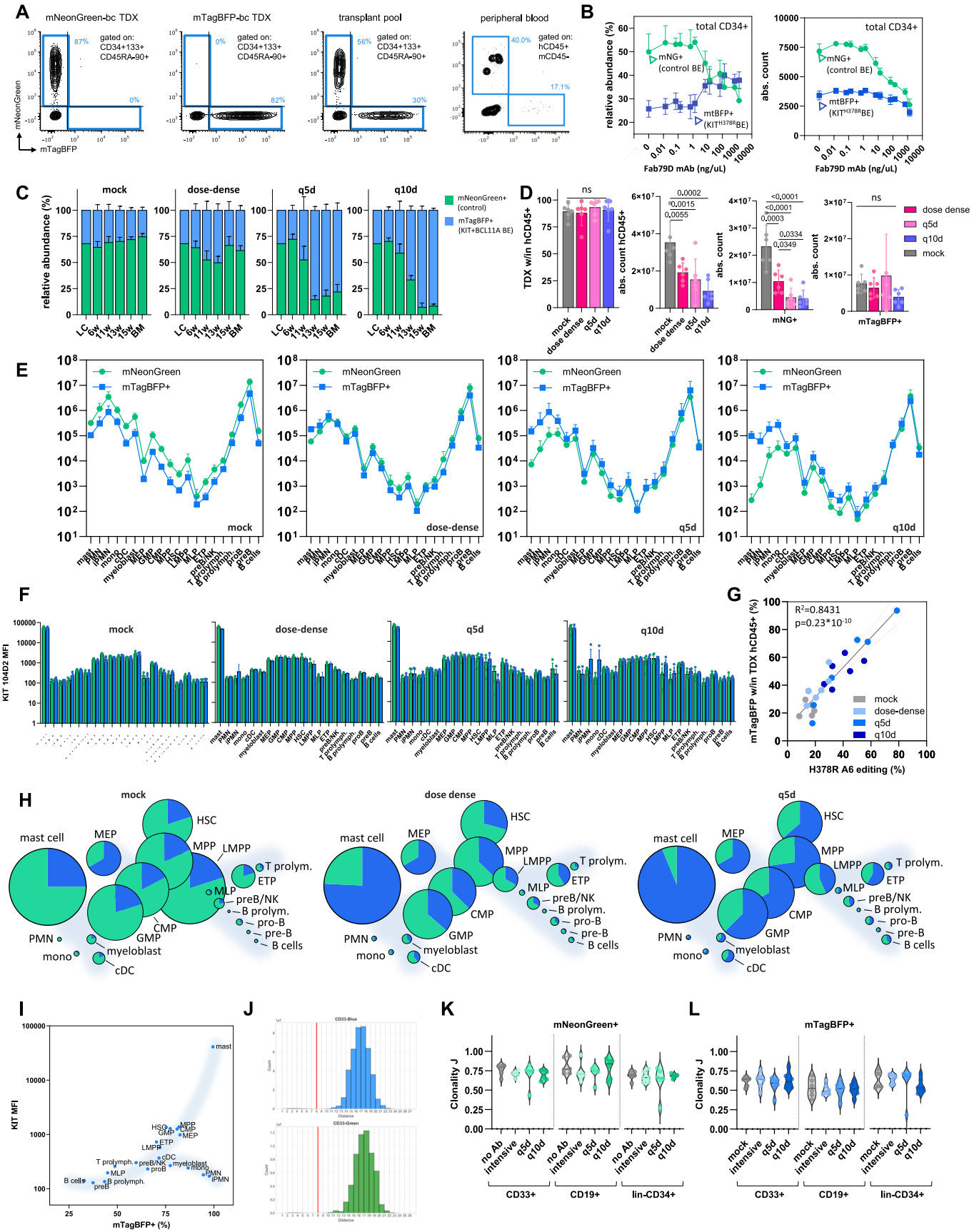

Extended Data Fig. 2 | See next page for caption.

Extended Data Fig. 2 | In vivo selection of KIT^{H378R} edited multilineage hematopoiesis following Fab-79D administration. (**A**) Representative flow cytometry plots showing fluorescent marking with mNeonGreen or mTagBFP by lentiviral transduction (TDX) of CD34+ HSPCs during in vitro expansion culture and after humanization in the PB of NBSGW mice from the experiment described in Fig. 2c (right-most plot). HSCs are pre-gated on the stem-enriched CD34+CD133+CD45RA-CD90+ fraction. (**B**) In vitro competitive selection experiment of KIT^{H378R} edited HSPCs (mTagBFP transduced, reported in blue) vs control-edited (mNeonGreen transduced, reported in green), cultured with different concentrations of Fab-79D mAb. Relative abundance (%, **left**) and absolute counts (**right**) of total CD34^{+} human cells. Mean ± SD. N = 4 replicates. (**C**) Relative abundance of mNeonGreen+ and mTagBFP+ cells within pre-transplant liquid culture (LC), peripheral blood (PB) timepoints (6w-15w), and BM at endpoint, across different Fab-79D dosing regimens (mock, dose-dense, q5d, q10d). This panel refers to the same in vivo competitive experiment described in Fig. 2c. Mean ± SD. N = 6 mice/group. (**D**) Left to Right: Lentiviral transduction (TDX) efficiency (%) within human CD45+ cells in the BM at endpoint across Fab-79D treatment; absolute counts of total hCD45+ cells within CD45+ in the BM; absolute counts of mNeonGreen^{+} (mNG) and mTagBFP^{+} (mtBFP) hCD45+ cells across Fab-79D treatment regimens. Mean ± SD. N = 6 mice/group. One-way ANOVA with multiple comparisons. This panel refers to the same in vivo competitive experiment described in Fig. 2c. One-way ANOVA. (**E**) Absolute counts of human hematopoietic subpopulations in the BM at endpoint, stratified by mTagBFP and mNeonGreen expression, across mock, dose-dense, q5d, and q10d Fab-79D treatment regimens. This panel refers to the same in vivo competitive experiment described in Fig. 2c. Mean ± SD. N = 6 mice/group. (**F**) KIT surface expression as Median Fluorescence Intensity (MFI) of KIT 104D2 antibody clone across hematopoietic subpopulations in the BM at endpoint for each treatment regimens. This panel refers to the same in vivo competitive experiment described in Fig. 2c. Mean ± SD. N = 6 mice/group. (**G**) Correlation of mTagBFP+ cells w/in TDX hCD45+ by flow (%) with KIT genomic editing efficiency at position A6 (%). Linear regression model statistics are reported within the plot. N = 6 mice/group. (**H**) Pie charts representing the outcomes of the in vivo selection across hematopoietic subsets in relation to the KIT surface expression by flow. Pie slice composition reports the proportion of mTagBFP+ versus mNeonGreen+ cells, while the radius of each pie is proportional to the KIT MFI. The q10d group is reported in Fig. 2f. N = 6 mice/group. (**I**) Correlation of KIT Median Fluorescence Intensity (MFI) by mTagBFP+ fraction in different hematopoietic subpopulations in the q10d treatment cohort. N = 6 mice/group. (**J**) Representative barplots reporting the pairwise UMI distance distributions used to define clustering thresholds. Levenshtein distances for the mTagBFP (**top**, blue) and mNeonGreen (**bottom**, green) barcode libraries. The cut-off used is highlighted by the red line. (**K**,**L**) Pielou's Evenness Index (**J**) in FACS-sorted myeloid (CD33+), lymphoid (CD19+), and progenitor (lineage-CD34+) compartments, within the mNeonGreen+ (**K**) and mTagBFP+ (**K**) fractions across treatment groups. N = 6 mice/group.

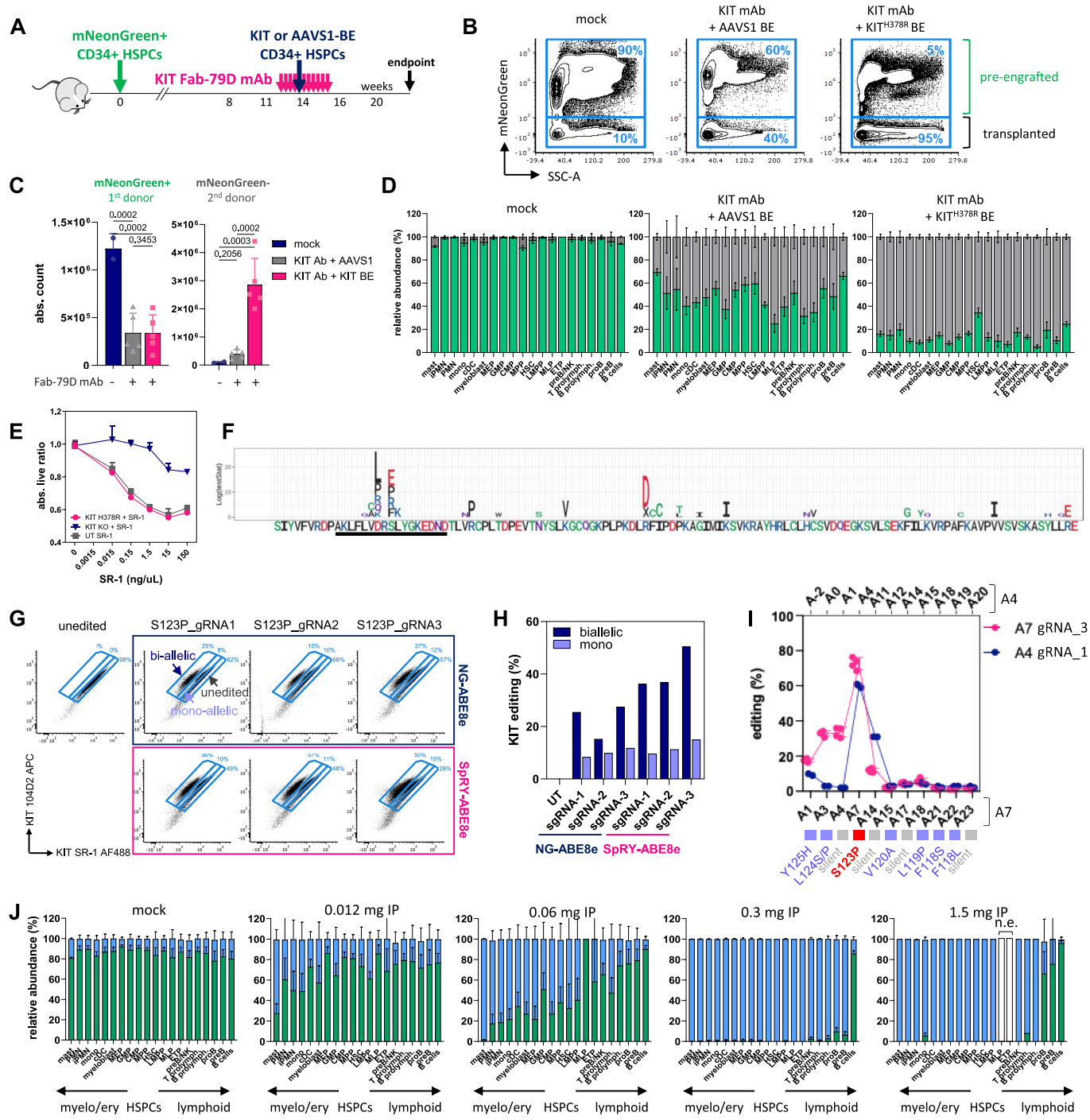

Extended Data Fig. 3 | See next page for caption.

Extended Data Fig. 3 | Enhanced hematopoietic replacement made possible by KIT^{H378R} epitope editing and optimization of KIT^{S123P} base editing for SR-1 shielding. (**A**) Experimental design to evaluate anti-KIT non-genotoxic conditioning and hematopoietic replacement. NBSGW mice were pre-engrafted with mNeonGreen LV-transduced (transduction efficiency 90%) unedited CD34+ HSPCs and, starting at week 12, conditioned with 8 doses of Fab-79D, followed by infusion of CD34+HSPCs from a second donor, either KIT^{H378R} or AAVS1 control base edited. N = 4 mice per group. (**B**) Representative flow cytometry plots showing the BM composition of human CD45+ cells by mNeonGreen fluorescence at endpoint, according to treatment group. (**C**) Absolute cell counts of mNeonGreen+ (pre-engrafted donor) and mNeonGreen- (transplanted second donor) human $CD45^+$ cells in the BM at endpoint. Mean ± SD. N = 4 mice per group. One-way ANOVA. (**D**) Relative composition (%) by mNeonGreen within hematopoietic subpopulations in the BM at endpoint, according to treatment group. mNeonGreen+ cells are reported in green, untransduced cells are reported in grey. Mean ± SD. N = 4 mice per group. (**E**) In vitro selection assay of CD34+ HSPCs cultured with different concentrations of SR-1 mAb in the presence of SCF showing orthogonality between the KIT^{H378R} epitope editing and SR-1 mAb mediated depletion. Absolute counts are normalized on SR-1 dose = 0. KIT knock-out (KO) cells show comparable counts to dose level = 0 due to loss of SCF-stimulated growth or inhibition. Mean ± SD. (**F**) Sequence logo showing the full range of the KIT ECD2 degenerated library (same as Fig. 3h). The axis reports the log-enrichment of amino acid substitutions in KIT 104D2+SR1- vs 104D2+SR+FACS-sorted fractions, compared to the wild-type sequence. The black bar highlights the range of the logo reported in Fig. 3h. (**G**) Representative flow cytometry plots of gRNA and BE screening to introduce the KIT^{S123P} mutation. 3 sgRNAs (columns) are tested in combination with 2 ABE8e variants (fused either with NG-Cas9n, blue outline; or SpRY-Cas9n, pink outline). Cells are co-stained with control clone 104D2 (y-axis) and SR-1 (x-axis). Gating identifies bi-allelic and mono-allelic edited cells. (**H**) Bar plots reporting the outcomes of the KIT^{S123P} BE screening reported in panel G, separated in mono- and biallelic editing. (**I**) Base editing efficiencies at different adenines within the window of KIT^{S123P} sgRNA_1 (A4) and sgRNA_3 (A7), with their respective A numbering reported above or below the plot. Bystander mutations are labelled with the possible codon changes below the plot. Mean ± SD. (**J**) Relative composition by fluorescence marking of mTagBFP+ and mNeonGreen+ populations across hematopoietic subsets within the BM at endpoint from the in vivo competitive selection experiment described in Fig. 3p. The cumulative SR-1 dose is reported above each plot. N.E., not evaluable due to low number of events. Mean ± SD. N = 4 mice/group.